Precision of the one-dimensional solutions for bonded double lap joints

PRECISION OF THE ONE-DIMENSIONAL SOLUTIONS FOR BONDED DOUBLE LAP JOINTS

L. Goglio*, M. Rossetto

Dipartimento di Meccanica, Politecnico di Torino

Corso Duca degli Abruzzi 24, 10129 Torino, Italy

Abstract

The solutions which have been proposed for the stress state in bonded joints inevitably adopt a simplified description. By comparison with finite element results, it can be noticed that the analytical solutions reproduce in general terms the stress field, but in the end zones of the overlap mismatches are frequently observed. The present paper focuses the attention on the double lap joint. The classical solutions found by Volkersen (Construction métallique 4, 1965) and Hart-Smith (Technical Report NASA CR-11234, 1973) are compared with a solution, developed in this work, which accounts for bending in the external adherends and axial stiffness imbalance. Several cases of adherend to adhesive elastic modulus ratio, thickness and overlap length are considered; finite element results are taken for reference. It is found that the analytical solutions give acceptable results when the elastic modulus of the adhesive is much lower than that of the adherends. The Volkersen's solution, although it fulfils the zero-traction boundary condition, does not give better results than the others and often underestimates the peak values. It is likely that a better description of stress variation through the adhesive thickness could improve substantially the situation.

Keywords: Double lap joint C. Stress analysis, Finite element stress analysis. E. Joint design.

---

*Corresponding author. Tel: +390115646934, Fax: +390115646999, E-mail: luca.goglio@polito.it

1 INTRODUCTION

Although, in present times, the stress-strain state in bonded joints can be completely assessed by means of finite element modelling, the need for analytical solutions is still alive. Indeed, apart from the scientific interest (equations can give a better insight of a phenomenon than numerical results alone), also from the designer's viewpoint formulae can be of quicker and simpler use for a first dimensioning of the joints (as for any structural part), leaving finite elements for a final analysis. The interest in this subject is also witnessed by the huge amount of research published over more than seven decades.

Looking back at the literature (see [1] for a recent survey) it appears that, after pioneering and fundamentals works as that of Goland and Reissner [2], who first accounted for both shear and peel stresses, the need for addressing some open issues was soon recognised. In general terms, the main aspects concern:

- the accuracy of the representation of the stress-strain state in the joint, especially in the adhesive;
- in case of a slender, single lap joint, the geometrical non-linearity due to the rotation.

Regarding the latter aspect, the initial idea by Goland and Reissner of treating the bonded overlap as a homogenous beam, to obtain the rotation and the moment acting at the overlap ends, was updated by the subsequent researchers. Renton and Vinson [3] extended the study to the case of orthotropic adherends. Hart-Smith [4] considered the two adherends as uncoupled and thus obtained considerably lower moment values, tending to zero in case of long overlaps, and also recognised an inconsistency in the free end of the adherends. The same correction was subscribed by Ojalvo and Eidinoff [5]. Later on, Oplinger [6] proposed another correction, leading to edge moment values closer to those of Goland and Reissner and very different from those of Hart-Smith in case of long overlaps. Tsai and Morton [7] compared the edge moments given by Goland and Reissner, Hart-Smith and Oplinger with results obtained from geometrically non-linear finite element analyses. Their conclusion was

that the Hart-Smith solution is best in case of short overlaps, whilst the Oplinger solution is best in case of long overlaps; however, the Goland and Reissner solution is reasonably accurate in all cases. More recently, Luo and Tong [8] developed a sophisticated non linear model, for which they found a (although complicated) closed-form solution, and which proved to give a better edge moment prediction than all previous models. Ultimately, Zhao *et al.* [9] proposed a simpler method for determining the end moments, which overcomes the limitation -shared by all models previously cited- of dealing with identical adherends. This method assumes that the overlap zone does not deform, and the authors found that the results are accurate as far as the overlap is not too long (length-to-thickness ratio up to 30).

Returning to the first of the two aspects listed above (i.e. the stress-strain state in the joint), the core of the problem is the inevitably simplified behaviour assumed for the adhesive and, to a lesser extent, also for the adherends. The classical description of the adhesive layer as distributed springs is incomplete, since only the peel and shear components of stress are considered; moreover, in this description these components are a function of the longitudinal coordinate only. Thus, neither the local, infinitesimal equilibrium, nor the natural boundary condition of zero traction on the free edges can be satisfied. Several proposals have been presented in the literature to remedy these shortcomings; a qualitative survey is given in this introduction, some analytical details are discussed in a following section.

In 1965, Volkersen [10] (in a study related to the double lap joint, but the idea is suitable in a general case) proposed to assume a simple linear variation of the peel stress through the thickness, which allows for fulfilling local equilibrium. The work of Hart-Smith [4] on single lap joints dealt mostly with the elasto-plastic failure modes, thus it was not concerned with improving the elastic solutions. Ojalvo and Eidinoff [5] used a complete relationship between shearing strain and displacement, which led to a definition of the shear stress variable through the thickness of the adhesive. Delale *et al.* [11], while extending the study of the lap joint to the case of orthotropic and shear-deformable adherends, considered also the longitudinal

strain -and, implicitly, the longitudinal stress- in the adhesive. However, the assumed stress state in the adhesive was still constant through the thickness and, therefore, unable to fulfil local equilibrium and boundary conditions. Adams and Mallick [12] developed a method, suitable for single and double lap joints, in which all stress components (shear, peel and longitudinal) in the adhesive are included and vary along the thickness. Their solution included six unknown functions of the longitudinal coordinate, and the problem was solved by minimization of the complementary energy (procedure implemented in an *ad hoc* software, JOINT). Another attempt to improve the solution was done by Tsai *et al.* [13]. In the case of double lap joint, they proposed a through-thickness triangular distribution for the shear stress in the external adherend (here referred to as gusset for sake of brevity, see also Fig. 1a), varying from zero (backface) to the adhesive shear stress (interface); bending in the gusset was neglected. In the case of single lap joints, they proposed two solutions: one treating the adherend as bars under tension, deforming also in shear; the other including bending. The adhesive was modelled as a spring layer, reacting with shear stresses only.

A more refined approach was given by the closed-form high-order theory developed by Frostig *et al*. [14]. In this approach it was deduced that, through the adhesive thickness, the shear stress must be constant, the peel stress varies linearly and the variation of the transverse displacement is quadratic; the longitudinal stress is neglected. Both local equilibrium and zero boundary conditions can be fulfilled by this stress state. In [15] Mortensen and Thomsen reported the formulation of a general method, implemented in the ESAComp software, in which the adherends are described as Kirchhoff plates and the adhesive is a spring layer transmitting peel and shear (in the two in-plane directions) stresses. The method was compared to closed-form high-order theory and finite element results, the authors remarked that the stresses predicted at the ends (not fulfilling the boundary conditions) could be regarded as conservative estimates of the actual stresses acting when spews are present at the overlap ends. Luo and Tuong [16] compared the behaviour of linear and higher order theories,

finding that in case of thick adhesive bondline the improvement given by the higher order is necessary. In recent times, Radice and Vinson [17] have developed another high-order elastic model, with the aim of clarifying the magnitude of the longitudinal stress and the actual stress-state (plane stress or plane strain) in the adhesive. The solution of the problem exhibits mathematical complications and is obtained as a series, by minimizing the potential energy functional. The conclusion of these authors is that the longitudinal stress in the adhesive is zero and that all other analytical or finite element models that find non-negligible longitudinal stress must be incorrect. Such a strong statement, practically denying all the related literature, should originate a considerable debate.

Very recently, Wang and Zhang [18] have presented a model in which the adhesive is formed by two normal spring layers, interfaced to the adherends, and an intermediate shear spring layer. With this conceptually simple modification, the transverse displacement of the adhesive mid plane is no longer the average of the two adherend transverse displacement and the peel stress is not constant through the thickness. As a consequence, the local equilibrium and the boundary conditions can be fulfilled.

Less work has been specifically dedicated to the case of the double lap joint. Apart from the paper by Volkersen [10] already mentioned above, the most known contribution is likely the Hart-Smith's report [19]. In that work, similarly to the companion report on single lap joints [4], most of the attention is focussed on the failure conditions; thus, due to adhesive plasticity, the shear stress at the ends of the overlap is assumed to be practically constant and the most relevant parameter is the strain energy to failure. However, the work recognises also the importance of the peel stresses, which can govern the failure in case of thick adherends. The Hart-Smith's elastic analysis, which neglects bending in the gussets, is recalled in short in a following section of the present paper.

Albat and Romilly [20] proposed a linear elastic solution, based on the Hart-Smith's solution, suitable to describe the stress state in double lap joints and also -due to its simplicity- in reinforcements made of stepped patches.

A much more sophisticated approach has been used by Bednarcyk *et al.* [21], Zhang *et al.* [22] who applied the "Higher Order Theory for Functionally Graded Materials" to the case of double lap joints and doubler joints. This theory is based on the discretization of the material in cells, within each of them the displacement field is approximated by a polynomial expansion, like in finite element modelling but without nodes. The approach can be regarded as an intermediate tool between analytical and finite element modelling; it has been implemented in a commercial software (Hypersizer®). Finally, another study of the orthotropic double lap joint has been presented in recent times by Gustafson *et al*. [23], who have solved with the virtual work principle two models of increasing sophistication: the first assumes shear stress only, while the second accounts for shear and peel components. Special end elements, called "end posts", are included to fulfil the zero-traction boundary condition.

At the end of this survey, a general remark is that models which are substantially the same as the first ones proposed several decades ago are still in use nowadays and coexist with more sophisticated and recent models. A first explanation for this is that closed-form solutions, which can be directly implemented at the level of a spreadsheet, are still appealing as a first design tool. If more complex, *ad hoc* programming is required (as it happens for those solutions based on minimization) the choice can easily turn in favour of finite element modelling. This is especially true in an industrial context, in which less time and expertise are available for mathematical or programming activities. A second explanation is that the sophisticated models, which fulfil the zero-traction boundary condition, nevertheless do not give the "exact" response in terms of peak stresses. Indeed, in most of the papers mentioned above the authors typically comment that the response of their models fits well the finite element results (the only that can be taken as a reference), except for the small regions close

to the overlap ends. Unfortunately, the main purpose of a stress analysis should be to predict stresses especially where they are more severe; if this is not the case, the mere fulfilment of the boundary condition is not so important for the designer. Another problem of all solutions which consider the through-thickness variability of the stresses is that they attempt to give a value also at the end of the adhesive-adherend interface, where the stress field is singular. Although several authors acknowledge this problem (e.g. [11],[12],[15],[16],[18],[23]), the only study accounting for the singularity in the through-thickness variability is that by Sawa *et al*. [24] which, however, involves a complicated mathematical solution that, again, implies the disadvantages of an *ad hoc* programming. In this perspective, it appears conceptually more appropriate to limit the comparison and the discussion to the situation on the adhesive mid plane.

The present paper deals with the case of the double lap joint, mainly to leave apart the aspects related to joint rotation and focus the attention on the description of the stress field in the adhesive mid plane. The goal is to evaluate the approximation on the peak stresses given by a one dimensional model, under different combinations of overlap length, adhesive thickness and elastic modulus ratio. The comparison is made with finite element results, and in one case also with strain gauge measurements on the gusset backface.

The paper is organised in the following way. First, some mathematical aspects concerning stress and strain in the adhesive are discussed, and the basic Hart-Smith solution is recalled. Second, the development of a more complete analytical model is explicitly presented. Then, the response obtained from the model is compared to finite element results. At the end, the conclusions and final remarks are presented.

2 MATHEMATICAL ASPECTS

This section presents some remarks concerning the different solutions listed above. Although the involved models have been stated several decades ago, it is instructive to reconsider some cases, noting the basic assumptions made by the different authors and their consequences on

the obtained stress state. For ease of comparison, symbols, reference axes, etc. are defined here in unique way, thus some formulae are reported in a different writing with respect to the corresponding original papers. It is assumed that *x* and *y* are, respectively, the longitudinal and transverse directions in the joint, the corresponding displacements are *u* and *v*, the stresses in the adhesive are τ_{xy} (shear), σ_y (peel) and σ_x (longitudinal).

It can be recalled first that the one dimensional models (Goland and Reissner [2] and similar), involve the two governing equations in the form

$$\frac{d^4\sigma_y}{dx^4} + A\sigma_y = 0; \qquad \frac{d^3\tau_{xy}}{dx^3} + B\frac{d\tau_{xy}}{dx} = 0 \tag{1a,b}$$

where *A*, *B* are constants. In case of dissimilar adherends (see e.g. [25]), such equations become non homogeneous and coupled, namely τ_{xy} appears in the right end side of Eq. (1a) and σ_y appears in the right end side of Eq. (1b). In this approach, these two stresses are a function of *x* only and σ_x is constantly nil; therefore, considering the local infinitesimal equilibrium equations

$$x \rightarrow: \frac{\partial\sigma_x}{\partial x} + \frac{\partial\tau_{xy}}{\partial y} = 0; \qquad y \uparrow: \frac{\partial\sigma_y}{\partial y} + \frac{\partial\tau_{xy}}{\partial x} = 0 \tag{2a,b}$$

the assumed stress state fulfils Eq. (2a) only.

2.1 Through-thickness variation of the stress: two opposite cases

In the work [10], Volkersen added to the peel stress a term varying linearly along the adhesive thickness, so that at the interfaces the peel stress is $\sigma_y \pm \sigma_r$. To fulfil Eq. (2b) it must be

$$\sigma_r = \frac{t}{2}\frac{d\tau_{xy}}{dx} \tag{3}$$

where *t* is the adhesive thickness. Furthermore, Volkersen considered an additional contribution γ to the adhesive shearing strain, related to the effect of the additional straining caused by σ_r (which is a function of *x*):

$$\gamma = -\frac{t}{4E_a}\frac{d\sigma_r}{dx} = -\frac{t^2}{8E_a}\frac{d^2\tau_{xy}}{dx^2} \tag{4}$$

where E_a is the adhesive Young's modulus. Thus, macroscopically, the relative longitudinal displacements between the two adherends is

$$\frac{u_1 - u_2}{t} = \frac{\tau_{xy}}{G_a} + \gamma = \frac{\tau_{xy}}{G_a} - \frac{t^2}{8E_a}\frac{d^2\tau_{xy}}{dx^2} \tag{5}$$

where u_1, u_2 are the displacements of the adherends (1,2) at the interfaces with the adhesive and G_a is the adhesive shear modulus. These assumptions originate a differential equation of the fifth order in the shear stress, see [10] Eq. (56), instead of the typical third order equation (Eq. (1b) or its equivalent):

$$\frac{d^5\bar{\tau}_{xy}}{dx^5} - \lambda_2^2\frac{d^3\bar{\tau}_{xy}}{dx^3} + u\lambda_3^4\frac{d\bar{\tau}_{xy}}{dx} = -v\lambda_3^4\bar{\sigma}_{xy} \tag{6}$$

where the constants λ_2, λ_3, u, v (note that here u and v are not displacements) are defined in the procedure and the bars simply indicate a normalization of the stresses. Having previously solved the peel stress, the solution of Eq. (6) is obtained by summing to the homogeneous solution a particular solution of the complete equation, related to the peel stress. The higher order of the problem allows fulfilling the condition of zero shear stress at the ends. The procedure is developed in the case of gussets as thick as half of the main (i.e. inner) adherend; unfortunately, in the article [10], several intermediate assumptions and simplifications are not reported explicitly, so that it is not possible to reconstruct easily the method in a general case. However, the Volkersen's assumption of peel stress varying through the thickness is valuable and is consistent with the high order theory developed years later [14].

A completely different approach was adopted by Ojalvo and Eidinoff [5], who started from the kinematic assumptions of displacements u, v varying linearly through the thickness:

$$u(x,y) = \frac{u_1 + u_2}{2} + \frac{u_1 - u_2}{t}y; \quad v(x,y) = \frac{v_1 + v_2}{2} + \frac{v_1 - v_2}{t}y \tag{7a,b}$$

where, again, u_i, v_i ($i = 1,2$) are the displacements of the adherends at the interfaces with the adhesive, which are a function of x only. It follows that the shearing strain in the adhesive is

$$\gamma_{xy} = \frac{\partial u}{\partial y} + \frac{\partial v}{\partial x} = \frac{u_1 - u_2}{t} + \frac{dv_1}{dx}\left(\frac{1}{2} + \frac{y}{t}\right) + \frac{dv_2}{dx}\left(\frac{1}{2} - \frac{y}{t}\right) \tag{8}$$

The first term in (8) is the usual "mean" shearing strain, appearing in most models, the following terms exhibit the dependence on y. As a consequence, the shear stress $\tau_{xy} = G_a \gamma_{xy}$ varies through the thickness. On the contrary, from Eq. (7b) it follows that the transverse direct strain is constant through the thickness

$$\varepsilon_{yy} = \frac{\partial v}{\partial y} = \frac{v_1 - v_2}{t} \tag{9}$$

and, therefore, also the peel stress $\sigma_y = E_a \varepsilon_y$ is constant. Thus this model does fulfil neither the longitudinal Eq. (2a), nor the transverse Eq. (2b) equilibrium. It is worth of note that none of the models proposed later in the literature adopted the assumptions of Ojalvo and Eidinoff.

2.2 Hart-Smith's solution for the double lap joint under axial load

The solution reported in [19]-Appendix A.1.1 for the elastic case assumes initially that the adherends are subjected to pure tension and the adhesive is subjected to shear stress and deforms consequently. Omitting here the thermal effects (included in the original work), the shear stress in the adhesive is

$$\tau_{xy} = G_a \gamma_{xy} = G_a \frac{u_1 - u_2}{t} \tag{10}$$

Differentiating Eq. (10) twice yields

$$\frac{d\tau_{xy}}{dx} = \frac{G_a}{t}\left(\frac{du_1}{dx} - \frac{du_2}{dx}\right) \tag{11}$$

$$\frac{d^2\tau_{xy}}{dx^2} = \frac{G_a}{t}\left(\frac{d^2u_1}{dx^2} - \frac{d^2u_2}{dx^2}\right) \tag{12}$$

Considering the deformability of the adherends it can be written

$$\frac{du_1}{dx} = \frac{T_1}{E_1 h_1}; \qquad \frac{du_2}{dx} = \frac{T_2}{E_2 h_2} \tag{13a,b}$$

where, respectively, T_1 and h_1 are the tensile force per unit width and thickness related to the gusset (index 1), T_2 and h_2 are the half tensile force per unit width and the half thickness related to the main adherend (index 2). Differentiating Eqs. (13a,b) yields

$$\frac{d^2u_1}{dx^2} = \frac{1}{E_1 h_1}\frac{dT_1}{dx}; \qquad \frac{d^2u_2}{dx^2} = \frac{1}{E_2 h_2}\frac{dT_2}{dx} \tag{14a,b}$$

The longitudinal equilibrium of the adherends implies that

$$\frac{dT_1}{dx} = \tau_{xy}; \qquad \frac{dT_2}{dx} = -\tau_{xy} \tag{15a,b}$$

By combining Eqs. (12), (14), (15) the following differential equation is obtained:

$$\frac{d^2\tau_{xy}}{dx^2} = \frac{G_a}{t}\left(\frac{1}{E_1 h_1} + \frac{1}{E_2 h_2}\right)\tau_{xy} \tag{16}$$

Terming $\lambda = \sqrt{\frac{G_a}{t}\left(\frac{1}{E_1 h_1} + \frac{1}{E_2 h_2}\right)}$, the solution of Eq. (16) can be rewritten in the form

$$\tau_{xy}(x) = B_1 e^{\lambda x} + B_2 e^{-\lambda x} \tag{17}$$

where B_1 and B_2 are integration constants which can be found by noting that at each end section of the overlap one of the forces T_1, T_2 vanishes and the other equals half of the total load carried by the joint.

To account also for the peel stress, Hart-Smith's analysis considers bending of the gusset. The related rotational and transverse equilibrium equations (Eqs. (64,65) in [19]) read:

$$\frac{dM}{dx} = V - \frac{h_1}{2}\tau_{xy}; \qquad \frac{dV}{dx} = -\sigma_y \tag{18a,b}$$

where M and V are, respectively, bending moment and shear force per unit width in the gusset. To eliminate the coupling with the shear stress introduced by Eq. (18a), Hart-Smith admits that in the end regions of the overlap the shear stress is practicallyconstant due to

adhesive plasticity. Thus, when Eq. (18a) is differentiated in the subsequent mathematical passages the shear stress disappears and the problem uncouples. This argument implies that the adhesive is in plastic regime regarding the shear stress and in elastic regime regarding the peel stress. It can be also remarked that, admitting bending in the gusset contradicts the displacement assumed in Eqs. (13a,b) to obtain the shear stress.

3 DOUBLE LAP JOINT MODEL

The model developed within this work considers a double lap joint (Fig. 1a) symmetrical with respect to its mid plane; the two gussets are identical but can be of any thickness and material. Due to the symmetry, the main (central) adherend is subjected to tension only, whilst the gussets undergo tension, shear and bending. For the reason stated at the end of the section 1, no attempt is made to account for the transverse variability of the shear stress τ_{xy} and the peel stress σ_y in the adhesive. The derivation of the model is very close to the procedure assumed by [25] for the single lap joint, the notation also has been kept similar for ease of comparison, the main difference being the behaviour (tension only) of the main adherend. Another difference is that the free body diagram assumed for equilibrium include, respectively, the upper or lower adherend and half of the adhesive thickness; this is consistent with considering the obtained solutions for the shear and peel stress as representative of the stress state in the mid-thickness plane of the adhesive layer.

3.1 Model equations

Considering Fig. 1b, the following equilibrium equations can be written for the gusset (subscript 1), involving axial force T_1, shear force V_1 and bending moment M_1 per unit width:

$$\frac{dT_1}{dx} - \tau_{xy} = 0 \tag{19}$$

$$\frac{dV_1}{dx} - \sigma_y = 0 \tag{20}$$

$$\frac{dM_1}{dx} - V_1 + \frac{h_1 + t}{2}\tau_{xy} = 0 \tag{21}$$

The longitudinal strain ε_{x1} at the inner surface of the gusset (interface with the adhesive) can be written as

$$\varepsilon_{x1} = \frac{du_1}{dx} = \frac{1-\nu_1^2}{E_1}\left(\frac{T_1}{h_1} - \frac{6M_1}{h_1^2}\right) \tag{22}$$

where u_1 is the longitudinal displacement, E_1 and ν_1 are respectively the Young's modulus and the Poisson's ratio of material 1. In addition, the usual relationship between curvature and bending moment can be written:

$$\frac{d^2 v_1}{dx^2} = -\frac{M_1}{D_1} \tag{23}$$

where v_1 is the transverse displacement and $D_1 = E_1 h_1^3 / 12(1-\nu_1^2)$ is the bending stiffness.

In a similar way, but considering only the tension, the following equations can be written for the main adherend (subscript 2), which involve axial force per unit width T_2 and strain ε_{x2} at the upper surface (interface with the adhesive):

$$\frac{dT_2}{dx} + \tau_{xy} = 0 \tag{24}$$

$$\varepsilon_{x2} = \frac{du_2}{dx} = \frac{1-\nu_2^2}{E_2}\frac{T_2}{h_2} \tag{25}$$

where u_2 is the longitudinal displacement, E_2 and ν_2 are respectively the Young's modulus and the Poisson's ratio of material 2.

The derivation of the first governing equation starts from the relationship between shear stress and relative longitudinal displacement:

$$\tau_{xy} = \frac{G_a}{t}(u_1 - u_2) \tag{26}$$

where G_a is the shear modulus of the adhesive. By differentiating Eq. (26) three times and considering Eqs. (19), (20), (21), (24), the shear stress can be related to the peel stress as follows:

$$\frac{d^3\tau_{xy}}{dx^3} - K_1\frac{d\tau_{xy}}{dx} = -K_2\sigma_y \tag{27}$$

where $K_1 = \frac{G_a}{t}\left[\frac{1-\nu_1^2}{E_1 h_1}\left(1+3\frac{h_1+t}{h_1}\right)+\frac{1-\nu_2^2}{E_2 h_2}\right]$, $K_2 = \frac{6G_a}{t}\frac{1-\nu_1^2}{E_1 h_1^2}$.

The second governing equation is obtained starting from the relationship between peel stress and transverse displacement of the gusset (as previously stated, the main adherend does not undergo transverse displacement):

$$\sigma_y = \frac{E_a}{(1-\nu_a^2)t} v_1 \tag{28}$$

where E_a and ν_a are, respectively the Young's modulus and the Poisson's ratio of the adhesive. It can be remarked that in writing Eq. (28) a plane strain condition in the adhesive has been assumed, unlike most of the known models which neglect the effect of the Poisson's ratio. By differentiating Eq. (28) four times and considering Eqs. (20), (21), (23), the peel stress can be related to the shear stress as follows:

$$\frac{d^4\sigma_y}{dx^4} + K_3\sigma_y = K_4\frac{d\tau_{xy}}{dx} \tag{29}$$

where $K_3 = \frac{E_a}{(1-\nu_a^2)tD_1}$, $K_4 = \frac{E_a(h_1+t)}{2(1-\nu_a^2)tD_1}$.

Since K_2 and K_4 can never be zero, Eqs. (27) and (29) are coupled; again as in [25] the problem is uncoupled by substituting Eq. (27) and its fourth derivative in Eq. (29), which gives:

$$\frac{d^7\tau_{xy}}{dx^7} - K_1\frac{d^5\tau_{xy}}{dx^5} + K_3\frac{d^3\tau_{xy}}{dx^3} - K_5\frac{d\tau_{xy}}{dx} = 0 \tag{30}$$

where $K_5 = K_1K_3 - K_2K_4$. Once the solution for τ_{xy} has been found, σ_y can be obtained from Eq. (27).

3.2 Solution and boundary conditions

Eq. (30) can be regarded as a sixth order differential equation, whose unknown function is the first derivative of τ_{xy}; searching the solution in exponential form $ae^{\lambda x}$, the following characteristic equation is found:

$$\lambda^6 - K_1\lambda^4 + K_3\lambda^2 - K_5 = 0 \tag{31}$$

Terming $\Lambda = \lambda^2$, the following third degree equation is obtained

$$\Lambda^3 - K_1\Lambda^2 + K_3\Lambda - K_5 = 0 \tag{32}$$

that admits one real root Λ_1 and two complex conjugate roots $\Lambda_{2,3} = X \pm \mathrm{i}Y$. Summarising, the six roots are:

$$\lambda_{1,2} = \pm\sqrt{\Lambda_1}\,, \qquad \lambda_{3,4} = \pm\sqrt{\Lambda_2} = \pm\sqrt{X + \mathrm{i}Y}\,, \qquad \lambda_{5,6} = \pm\sqrt{\Lambda_3} = \pm\sqrt{X - \mathrm{i}Y}$$

and the unknown function is in the form (in which a_1-a_6 indicate generic constants):

$$\frac{d\tau_{xy}}{dx} = a_1 \mathrm{e}^{+\sqrt{\Lambda_1}x} + a_2 \mathrm{e}^{-\sqrt{\Lambda_1}x} + a_3 \mathrm{e}^{+\sqrt{X+\mathrm{i}Y}x} + a_4 \mathrm{e}^{-\sqrt{X+\mathrm{i}Y}x} + a_5 \mathrm{e}^{+\sqrt{X-\mathrm{i}Y}x} + a_6 \mathrm{e}^{-\sqrt{X-\mathrm{i}Y}x} \tag{33}$$

A further additional integration is required to obtain τ_{xy}, but, thanks to the exponential form of the terms, the only practical consequence on the structure of the solution is that of adding a constant. Thus, terming the new constants C_1-C_7, the solution can be written as:

$$\begin{aligned}\tau_{xy} = {} & C_1 \cosh(m_1 x) + C_2 \sinh(m_1 x) + C_3 \cosh(n_1 x)\cos(n_2 x) + C_4 \cosh(n_1 x)\sin(n_2 x) + \\ & + C_5 \sinh(n_1 x)\cos(n_2 x) + C_6 \sinh(n_1 x)\sin(n_2 x) + C_7\end{aligned} \tag{34}$$

Explicit formulae for the coefficients m_1, n_1, n_2 are given in Appendix. The determination of C_1-C_7 is based on the edge loads applied at the ends of the bond, shown in Fig. 1c (subcripts *l*, *r* indicate the left, right end). At the right end of the gusset and at the left end of the main adherend (free ends) all loads are obviously zero; at the right end of the (half) main adherend the axial load per unit width is $P/2$, as well as at the left end of the gusset. Regarding the latter condition, usually in the literature [10],[13],[19],[20] only the presence of the axial load is considered. In [26] it was recognized that, due to the offset between the line of action of the axial load in the gusset and the resultant of the shear stress transmitted by the adhesive, a bending action can arise, as schematized in Fig. 2. By simple arguments, based on symmetry and equilibrium, it can be noticed that in the unbonded length of the gusset the shear force is certainly zero and a constant bending moment, of unknown value, can exist. The latter is the

moment M_{1l} that in this work is regarded as a further unknown, in addition to C_1-C_7; therefore, eight conditions are required in total.

The first six of these are obtained as three pairs, by evaluating equations based on the derivatives of τ_{xy} both in $x = 0$ and in $x = L$.

- conditions 1), 2)

$$\frac{d\tau_{xy}}{dx} = \frac{G_a}{t}\left[\frac{1-\nu_1^2}{E_1}\left(\frac{T_1}{h_1} - \frac{6M_1}{h_1^2}\right) - \frac{1-\nu_2^2}{E_2}\frac{T_2}{h_2}\right] \tag{35a,b}$$

- conditions 3), 4)

$$\frac{d^5\tau_{xy}}{dx^5} - K_1\frac{d^3\tau_{xy}}{dx^3} = K_2\frac{E_a}{(1-\nu_a^2)t}\frac{M_1}{D_1} \tag{36a,b}$$

- conditions 5), 6)

$$\frac{d^6\tau_{xy}}{d^6x} - K_1\frac{d^4\tau_{xy}}{d^4x} + K_2\frac{E_a(h_1+t)}{2(1-\nu_a^2)tD_1}\tau_{xy} = 0 \tag{37a,b}$$

The two remaining conditions are obtained by considering respectively the longitudinal and rotational equilibrium of the gusset:

- condition 7)

$$\int_0^L \tau_{xy}dx = -P/2 \tag{38a}$$

- condition 8)

$$\int_0^L \sigma_{xy}xdx = \int_0^L\left(-\frac{1}{K_2}\frac{d^3\tau_{xy}}{dx^3} + \frac{K_1}{K_2}\frac{d\tau_{xy}}{dx}\right)xdx = M_{1l} + \frac{P}{2}\frac{h_1+t}{2} \tag{38b}$$

The set of eight conditions is rewritten in matrix form

$$[A]\{X\} = \{B\} \tag{39}$$

where [A] is the 8×8 coefficient matrix, vector {B} contains the known terms (related to P) and vector {X} contains the unknown constants C_1-C_7, M_{1l}. The definitions of all terms of [A] and {B} are given explicitly in Appendix. Although the expressions are long, the set of equation (39) can be easily implemented and solved, even by means of a spreadsheet.

4 RESULTS

4.1 Comparison between analytical solutions

An initial comparison has been carried between the solution for the double lap joint developed in this paper and the most significant literature solutions, namely those by Volkersen [10] and Hart-Smith [19]. For the application of the latter, instead of uncoupling the peel from the shear stress as done in the original work, the peel stress has been obtained from the shear stress given by Eq. (17) by means of Eq. (27) (for this reason such stress is labelled "adapted" in the related graphs). Three sample cases have been considered, in the first ("stiff" adherend) the ratio $E_{\text{adher}} / E_{\text{adhes}}$ (the elastic moduli of adherend and adhesive respectively) is equal to 100, e.g. as for a steel / epoxy bond, in the second ("intermediate" adherend) this ratio equals 20, e.g. as for a composite / epoxy bond, in the third ("soft" adherend) the ratio equals 5, e.g. as for a reinforced polymer / epoxy bond. In all cases, the Poisson's ratio of the adhesive is 0.4, that of the adherends 0.29. The thickness of the gusset h_1 and the half-thickness of the main adherend h_2 are 1.5 mm, the thickness of the adhesive layer t is 0.25 mm, the overlap length is 30 mm. This length value is high enough to distinguish the behaviours of the different solutions, but not so high to cause numerical troubles to the calculation of the hyperbolic and harmonic functions appearing in the solutions. The applied loading corresponds to an average shear stress of 1 MPa in the adhesive. Fig. 3a shows the stresses in the adhesive mid-plane in the case of "stiff" adherend material. Regarding the shear stress, it can be noticed that the Volkersen's solution drops to zero at the ends, fulfilling the boundary conditions, whilst the remaining solutions do not. In comparison, the Hart-Smith's solution gives higher values at the ends (peaks) and lower values in the middle; the solution developed in this paper is generally between the other two. Regarding the peel stress, the three solutions give similar answers; the peaks of the Volkersen's solution are slightly lower.

The situation already changes noticeably in case of "intermediate" adherend material shown in Fig. 3b, where the stress peaks are approximately double than in the previous case. The

shear stresses predicted by the three solutions are clearly different; the Volkersen's solution gives peaks which are lower than the solution developed in this paper, which is, in turn, lower than that of Hart-Smith. For the peel stress the Volkersen's solution gives values slightly lower than the other two.

A further change occurs in the case of "soft" adherend material, shown in Fig. 3c; here the highest stress peaks reach about 10 times the average stress. Regarding the shear stresses, the Volkersen's solution gives peaks which are less than half of the other two solutions; again, the Hart-Smith's solution gives the highest prediction. Conversely, for the peel stress the three solutions give similar results, also in this case the Volkersen's solution gives values slightly lower than the other two.

An additional result of the solution developed in this paper is that the bending moment in the gusset at its loaded end (M_{1l}, here treated as an unknown) is nil, this confirms the assumption usually adopted by the other solutions of the literature.

4.2 Comparison with finite element results

A large part of this work concerned the comparison of the analytical predictions with finite element results, in a series of cases which includes different combinations of overlap length, adhesive thickness and elastic modulus ratio. Keeping constant the gusset thickness (1.5 mm) and the main adherend thickness (2×1.5 mm), the remaining parameters have been varied as follows:

- elastic modulus ratio E_{adher} / E_{adhes} = 100, 20, 5; the Poisson's ratio of the adhesive is 0.4, that of the adherends 0.29 (as in the previous section);
- adhesive thickness t = 0.25, 0.50 mm;
- overlap length L = 10, 30, 50 mm in the case of "stiff" adherend material, L = 10, 20, 30 mm in the case of "intermediate" and "soft" adherend material (in these cases the

eigenvalues m_1, n_1 and n_2 are larger, thus the numerical troubles concerning the hyperbolic and harmonic functions start to appear at lower values of L).

In relative terms, the combinations of thickness and length can be regarded as $t/h_1 = 1/6,\ 1/3$ and $L/h_1 = 20/3,\ 20,\ 100/3$ for the "stiff" adherend, $L/h_1 = 20/3,\ 40/3,\ 20$ for the "soft" adherend.

The finite element models have been built using 8 node isoparametric elements in plane strain conditions; the minimum element size for the adhesive (and for the zones of the adherends near to the bond) is 0.05 mm. It has been found by comparison with more refined meshes that this size is enough for the scope of this work; obviously a much smaller size (10^{-5} mm) would be required to describe the singularity at the interface end [27]. A detail view of the mesh is shown in Fig. 4.

Fig. 5 show, as an example, the stress distribution in the mid plane of the adhesive in the case $E_{\text{adher}} / E_{\text{adhes}} = 100$ and $t = 0.25$, for all considered overlaps. The stress distributions given by the solution developed in this paper and the Volkersen's solution are compared to the finite element results. As far as the shear stress is concerned, the solution developed here, although simpler than that of Volkersen, reproduces quite well the finite element results, also for the maxima, even if the boundary condition is not fulfilled. For the longest overlap the Volkersen's solution underestimates the peak value. Regarding the peel stress, the two solutions are almost indistinguishable; none of them can reproduce the fall of the curve given by finite element at the overlap end. The same graphs report also the distribution of the longitudinal stress σ_x; it can be noticed that this component is smaller than the other two, but is not actually negligible (about one half of the peel stress σ_y).

The rather different situation of the case $E_{\text{adher}} / E_{\text{adhes}} = 5$ and $t = 0.25$, again for all considered overlaps, is shown in Fig. 6. It is apparent that the stress distribution given by the finite element model is markedly non-symmetric from left to right: at the left end (where the

main adherend is loaded and the gusset is unloaded) the stresses are lower. Moreover, the longitudinal stress is no longer nil in the central zone of the bondline. The analytical solutions still predict a symmetric distribution; therefore, at the left end the error is high (only the Volkersen's solution behaves better). Also along the overlap the related graphs do not reproduce accurately the finite element results.

A synthesis of the results corresponding to all cases is reported in Tabs. 1-3, which contain the peak values of peel and shear stress given by analytical solutions and finite element models, as well as their relative difference expressed in percent (the difference is positive when the solution overestimates, and negative when underestimates, in absolute value, the finite element results). In general terms, the analytical solutions approximate the shear stress better than the peel stress and the situation at the right end better than that at the left end. In the case $E_{\text{adher}} / E_{\text{adhes}} = 100$ (Tab. 1) the difference reaches 18% and -19.1% for the peak peel stress. For the peak shear stress in most cases the difference is of some unit percent, but the Volkersen's solution exhibits differences around -15.3% and -17.6% in the case $L = 50$ mm. The situation progressively worsens in the cases $E_{\text{adher}} / E_{\text{adhes}} = 20$ (Tab. 2) and $E_{\text{adher}} / E_{\text{adhes}} = 5$ (Tab. 3), for which the difference of the left peak peel stress respectively exceeds 50% and almost attains 150%. The estimate of the right peak shear stress is never so poor, but the Volkersen's solutions gives the highest differences, namely -16.6% and -45.5% instead of 6.4% and 22.9% given by the solution developed in this work, respectively for elastic modulus ratio equal to 20 and 5.

Therefore, it can be remarked that, even if the Volkersen's solutions appears conceptually more satisfactory for it fulfils the boundary condition, the results that it gives are in many instances worse and underestimate the peak stress.

4.3 Comparison with experimental measurements

A specimen formed by a double lap joint, with characteristic dimensions $h_1 = h_2 = 1.5$ mm, $t = 0.50$ mm, $L = 30$ mm, has been prepared from sheets of structural steel bonded with

adhesive Hysol 9466 (Henkel Loctite, Düsseldorf, Germany) and instrumented with strain gauges (Fig. 7). The gussets have been manufactured long enough to allow for a central unbonded length of 80 mm (between the unloaded ends of the main adherends), to allow space for placing a pair of gauges (one at mid-span and another at quarter-span) on the outer surface of a gusset and, correspondingly, another pair on the inner surface. A chain of longitudinal strain gauges with 10 elements and pitch 1 mm has been applied on the backface of a gusset in the bonded zone. The specimen has been suspended vertically and loaded axially with known weights.

Tab. 4 reports the strain obtained from the gauges (mean of two measurements) in the unbonded zone of the gusset and the theoretical value corresponding to a state of pure tension, at the loading level 30 N/mm. The slight differences among the measurements are likely due to the experimental error, thus the state of pure tension in the gusset is confirmed. Fig. 8 shows the values of longitudinal strain measured by the strain gauge chain on the back face of the gusset, compared to the strain distribution given by the finite element results and the solution developed in this work. In addition, also the strain distribution obtained by considering only the membrane behaviour of the gusset is plotted for comparison. Although some of the experimental values appear slightly lower than expected, the agreement is more than satisfactory. Finally, it is apparent that ignoring the effect of gusset bending (as, in practice, assumed by the Hart-Smith solution) leads to ignore the peaks at the ends of the overlap.

4.4 Cases of stiffness unbalance

The study has been extended also to cases in which (keeping the symmetry of the joints) the main adherend is no longer thick twice the gusset and the materials of the adherends are different. Thus, the axial stiffness of the main adherend differs from the sum of the stiffness of the two gussets; it is known [19] that in such a case the adhesive is more stressed at the overlap end corresponding to the loaded end of the less stiff adherend. Fig. 9 shows the stress

distribution in the adhesive mid-plane for the two cases of unbalance ratio $E_1h_1 / E_2h_2 = 2.3$, and $E_1h_1 / E_2h_2 = 0.4$. The elastic modulus ratios (adherend to adhesive) are approximately 19 and 34; the adhesive thickness and bond length are always 0.25 mm and 30 mm respectively. It is apparent that the analytical solution developed here (note that in these cases the Volkersen's solution is not available) reproduces generally well the finite element results, but a relevant discrepancy occurs at the left end. Tab. 5 reports the peak values and the relative difference, the inaccuracy concerns the peel stress (40-50%) and, to a lesser extent, the shear stress (around 15%). It is interesting to notice that the problems occur once again at the left end, independently of the unbalance ratio, i.e. independently of where the stresses are highest.

5 CONCLUSIONS

The performance of a one dimensional solution for the double lap joint -accounting for bending of the gussets- has been compared to the corresponding Volkersen's solution (not available in case of stiffness unbalance) and to finite element results.

- The analytical solutions give acceptable results when the elastic modulus of the adhesive is much lower than that of the adherends; this can be explained by the fact that when the elastic moduli are comparable the description of the adhesive as a spring layer is no longer adequate.
- The Volkersen's solution, to fulfil the zero traction boundary condition, assumes a linear through-thickness variation of the peel stress. However, the results for the stresses in the mid plane that it gives are not better that those of the one dimensional solution and they often underestimate the values.
- Considering the literature, an issue that still has not been addressed is how to include properly (keeping the description of the adherends as plates) the through-thickness variation of the stresses, accounting also for the problem of the stress singularity at the end of the adhesive / adherend interface. The linear variation that has been adopted by

several authors (including Volkersen) is not sufficient, in the sense that it merely fulfils local equilibrium and boundary condition, but it does not give correct results, neither for the peak, nor for the interface end. It is likely that an advance regarding this topic could improve the description of the stress distribution at the ends of the overlap and fulfil the boundary condition as well.

6 ACKNOWLEDGEMENTS

The authors thank Mr Lotfi Garai (visiting student from ENSTA - Paris) for his contribution to the development of the mathematical model and for the strain gauge installation.

7 REFERENCES

[1] L.F.M. da Silva, P.J.C. das Neves, R.D. Adams, J.K. Spelt, Analytical models of adhesively bonded joints – Part I: Literature survey, Int. J. Adhes. Adhes. 29 (2009) 319-330.

[2] M. Goland, E. Reissner, The stresses in cemented joints, J Appl. Mech. 66 (1944) A17-A27.

[3] W.J. Renton, J.R. Vinson, Analysis of adhesively bonded joints between panels of composite materials, J. Appl. Mech. 44 (1977) 101-107.

[4] L.J. Hart-Smith, Adhesive-bonded single-lap joints, Technical Report NASA CR-11236, 1973.

[5] I.U. Ojalvo, H.L. Eidinoff, Bond thickness effects upon stresses in single-lap adhesive joints, AIAA J. 16(3) (1978) 204-211.

[6] D.W. Oplinger, Effects of adherend deflections in single lap joints, Int. J. Sol. Struct. 31 (1994) 2565-2587.

[7] M.Y. Tsai, J. Morton, An evaluation of analytical and numerical solutions to the single-lap joint, Int. J. Sol. Struct. 31 (1994) 2537-2563.

[8] Q. Luo, L. Tong, Fully-coupled non linear analysis of single lap adhesive joints, Int. J.

Sol. Struct. 44 (2007) 2349-2370.

[9] X. Zhao, R.D. Adams, Lucas F.M. da Silva, A new method for the determination of bending moments in single lap joints, Int. J. Adhes. Adhes. 30 (2010) 63-71.

[10] O. Volkersen, Recherches sur la théorie des assemblages collés, Construction métallique 4 (1965) 3-13.

[11] F. Delale, F. Erdogan, M.N. Aydinoglu, Stresses in adhesively bonded joints: a closed form solution, J. Compos. Mater. 15 (1981) 249-271.

[12] R.D. Adams, V. Mallick, A method for the stress analysis of lap joints, J. Adhesion 38 (1992) 199-217.

[13] M.Y. Tsai, D.W. Oplinger, J. Morton, Improved theoretical solutions for adhesive lap joints, Int. J. Sol. Struct. 35 (1998) 1163-1185.

[14] Y. Frostig, O.T. Thomsen, F. Mortensen, Analysis of adhesive-bonded joints, square-end and spew-fillet − High-order theory approach, J. Eng. Mech.-ASCE 125 (1999) 1298-1307.

[15] F. Mortensen, O.T. Thomsen, Analysis of adhesive bonded joints: a unified approach, Compos. Sci. Technol. 62 (2002) 1011-1031.

[16] Q. Luo, L. Tong, Linear and higher order displacement theories for adhesively bonded lap joints, Int. J. Sol. Struct. 41 (2004) 6351-6381.

[17] J.J. Radice, J.R Vinson, On the analysis of adhesively bonded structures: a high order semi-elastic adhesive layer model, Compos. Sci. Technol. 68 (2008) 376-386.

[18] J. Wang, C. Zhang, Three-parameter, elastic foundation model for analysis of adhesively bonded joints, Int. J. Adhes. Adhes. 29 (2009) 495-502.

[19] L.J. Hart-Smith, Adhesive-bonded double-lap joints, Technical Report NASA CR-11234, 1973.

[20] A.M. Albat, D.P. Romilly, A direct linear-elastic analysis of double symmetric bonded joints and reinforcements, Compos. Sci. Technol. 59 (1999) 1127-1137.

[21] B.A. Bednarcyk, J. Zhang, C.S. Collier, Y. Bansal, M.-J. Pinder, Analysis tools for adhesively bonded composite joints, part 1: higher-order theory, AIAA J. 44(1) (2006) 171-180.

[22] J. Zhang, B.A. Bednarcyk, C.S. Collier, P. Yarrington, Y. Bansal, M.-J. Pinder, Analysis tools for adhesively bonded composite joints, part 2: unified analytical theory, AIAA J. 44(8) (2006) 1709-1719.

[23] P.A. Gustafson, A. Bizard, A.M. Waas, Dimensionless parameters in symmetric double lap joints: an orthotropic solution for thermomechanical loading, Int. J. Sol. Struct. 44 (2007) 5774-5795.

[24] T. Sawa, J. Liu, K. Nakano, J. Tanaka, A two-dimensional stress analysis of single-lap adhesive joints of dissimilar adherends subjected to tensile loads, J. Adhes. Sci. Technol. 14 (2000) 43-66.

[25] D.A. Bigwood, A.D. Crocombe, Elastic analysis and engineering design formulae for bonded joints, Int. J. Adhes. Adhes. 9 (1989) 229-242.

[26] R.D. Adams, J. Comyn, W.C. Wake, Structural adhesive joints in engineering, London: Chapman & Hall; 1997.

[27] L. Goglio, M. Rossetto, Stress intensity factor in bonded joints: influence of the geometry, Int. J. Adhes. Adhes. 30 (2010) 313-321.

APPENDIX

- Roots of the characteristic equation (31)

$$m_1 = \sqrt{\frac{C^{1/3}}{3\cdot 2^{1/3}} + \frac{K_1}{3} - \frac{2^{1/3}\left(-K_1^2 + 3K_3\right)}{3C^{1/3}}}$$

$$n_1 = \sqrt[4]{X^2 + Y^2}\cos\left(\frac{1}{2}\arccos\left(\frac{X}{\sqrt{X^2 + Y^2}}\right)\right)$$

$$n_2 = \sqrt[4]{X^2+Y^2}\,\sin\left(\frac{1}{2}\arccos\left(\frac{X}{\sqrt{X^2+Y^2}}\right)\right)$$

where

$$C = 2K_1^3 - 9K_1K_3 + 27K_5 + \sqrt{-4\left(K_1^2-3K_3\right)^3 + \left(2K_1^3 - 9K_1K_3 + 27K_5\right)^2}\,,$$

$$X = \frac{-2^{2/3}C^{2/3} + 4C^{1/3}K_1 - 2\cdot 2^{1/3}K_1^2 + 6\cdot 2^{1/3}K_3}{12C^{1/3}}, \quad Y = \frac{2^{1/3}C^{2/3} - 2K_1^2 + 6K_3}{2\cdot 2^{2/3}\sqrt{3}C^{1/3}}$$

- Equation set (39): coefficients a_{ij} of matrix [A] and b_j of vector {B} (i,j = 1,..,8)

$a_{11} = 0$, $a_{12} = m_1$, $a_{13} = 0$, $a_{14} = n_2$, $a_{15} = n_1$, $a_{16} = 0$, $a_{17} = 0$,

$a_{18} = \frac{G_a}{t}\frac{6\left(1-\nu_1^2\right)}{E_1h_1^2}$, $b_1 = \frac{G_a}{t}\frac{1-\nu_1^2}{E_1h_1}\frac{P}{2}$;

$a_{21} = m_1\sinh(m_1L)$, $a_{22} = m_1\cosh(m_1L)$, $a_{23} = n_1\cos(n_2L)\sinh(n_1L) - n_2\sin(n_2L)\cosh(n_1L)$

, $a_{24} = n_1\sin(n_2L)\sinh(n_1L) + n_2\cos(n_2L)\cosh(n_1L)$,

$a_{25} = n_1\cos(n_2L)\cosh(n_1L) - n_2\sin(n_2L)\sinh(n_1L)$,

$a_{26} = n_1\sin(n_2L)\cosh(n_1L) + n_2\cos(n_2L)\sinh(n_1L)$, $a_{27} = 0$, $a_{28} = 0$,

$b_2 = -\frac{G_a\left(1-\nu_2^2\right)}{tE_2h_2}\frac{P}{2}$;

$a_{31} = 0$, $a_{32} = -K_1m_1^3 + m_1^5$, $a_{33} = 0$, $a_{34} = 5n_1^4n_2 - 10n_1^2n_2^3 + n_2^5 - K_1\left(3n_1^2n_2 - n_2^3\right)$,

$a_{35} = n_1^5 - 10n_1^3n_2^2 + 5n_1n_2^4 - K_1\left(n_1^3 - 3n_1n_2^2\right)$, $a_{36} = 0$, $a_{37} = 0$, $a_{38} = \frac{E_aK_2}{t(1-\nu_a^2)D_1}$, $b_3 = 0$;

$a_{41} = \sinh(m_1L)\left(-K_1m_1^3 + m_1^5\right)$, $a_{42} = \cosh(m_1L)\left(-K_1m_1^3 + m_1^5\right)$,

$$a_{43} = \cos(n_2L)\sinh(n_1L)\left(-K_1n_1^3 + n_1^5 + 3K_1n_1n_2^2 - 10n_1^3n_2^2 + 5n_1n_2^4\right) + \sin(n_2L)\cosh(n_1L)\left(3K_1n_1^2n_2 - 5n_1^4n_2 - K_1n_2^3 + 10n_1^2n_2^3 - n_2^5\right),$$

$$a_{44} = \sin(n_2L)\sinh(n_1L)\left(-K_1n_1^3 + n_1^5 + 3K_1n_1n_2^2 - 10n_1^3n_2^2 + 5n_1n_2^4\right) + -\cos(n_2L)\cosh(n_1L)\left(3K_1n_1^2n_2 - 5n_1^4n_2 - K_1n_2^3 + 10n_1^2n_2^3 - n_2^5\right),$$

$$a_{45} = \cos(n_2L)\cosh(n_1L)\left(-K_1n_1^3 + n_1^5 + 3K_1n_1n_2^2 - 10n_1^3n_2^2 + 5n_1n_2^4\right) + \sin(n_2L)\sinh(n_1L)\left(3K_1n_1^2n_2 - 5n_1^4n_2 - K_1n_2^3 + 10n_1^2n_2^3 - n_2^5\right),$$

$$a_{46} = \sin(n_2 L)\cosh(n_1 L)\left(-K_1 n_1^3 + n_1^5 + 3K_1 n_1 n_2^2 - 10 n_1^3 n_2^2 + 5 n_1 n_2^4\right) + \\ -\cos(n_2 L)\sinh(n_1 L)\left(3K_1 n_1^2 n_2 - 5 n_1^4 n_2 - K_1 n_2^3 + 10 n_1^2 n_2^3 - n_2^5\right),$$

$$a_{47} = 0, \quad a_{48} = 0, \quad b_4 = 0;$$

$$a_{51} = -K_1 m_1^4 + m_1^6 + \frac{E_a (h_1 + t) K_2}{2t(1-\nu_a^2) D_1}, \quad a_{52} = 0,$$

$$a_{53} = n_1^6 - 15 n_1^4 n_2^2 + 15 n_1^2 n_2^4 - n_2^6 - K_1\left(n_1^4 - 6 n_1^2 n_2^2 + n_2^4\right) + \frac{E_a (h_1 + t) K_2}{2t(1-\nu_a^2) D_1}, \quad a_{54} = 0, \quad a_{55} = 0,$$

$$a_{56} = 6 n_1^5 n_2 - 20 n_1^3 n_2^3 + 6 n_1 n_2^5 - 4K_1\left(n_1^3 n_2 - n_1 n_2^3\right), \quad a_{57} = \frac{E_a (h_1 + t) K_2}{2t(1-\nu_a^2) D_1}, \quad a_{58} = 0, \quad b_5 = 0;$$

$$a_{61} = \cosh(m_1 L)\left(-K_1 m_1^4 + m_1^6 + \frac{E_a (h_1 + t) K_2}{2t(1-\nu_a^2) D_1}\right),$$

$$a_{62} = \sinh(m_1 L)\left(-K_1 m_1^4 + m_1^6 + \frac{E_a (h_1 + t) K_2}{2t(1-\nu_a^2) D_1}\right),$$

$$a_{63} = \sin(n_2 L)\sinh(n_1 L)\left(4K_1 n_1^3 n_2 - 6 n_1^5 n_2 - 4K_1 n_1 n_2^3 + 20 n_1^3 n_2^3 - 6 n_1 n_2^5\right) + \\ \cos(n_2 L)\cosh(n_1 L)\left(-K_1 n_1^4 + n_1^6 + 6K_1 n_1^2 n_2^2 - 15 n_1^4 n_2^2 - K_1 n_2^4 + 15 n_1^2 n_2^4 - n_2^6 + \frac{E_a (h_1 + t) K_2}{2t(1-\nu_a^2) D_1}\right),$$

$$a_{64} = -\cos(n_2 L)\sinh(n_1 L)\left(4K_1 n_1^3 n_2 - 6 n_1^5 n_2 - 4K_1 n_1 n_2^3 + 20 n_1^3 n_2^3 - 6 n_1 n_2^5\right) + \\ \sin(n_2 L)\cosh(n_1 L)\left(-K_1 n_1^4 + n_1^6 + 6K_1 n_1^2 n_2^2 - 15 n_1^4 n_2^2 - K_1 n_2^4 + 15 n_1^2 n_2^4 - n_2^6 + \frac{E_a (h_1 + t) K_2}{2t(1-\nu_a^2) D_1}\right),$$

$$a_{65} = \sin(n_2 L)\cosh(n_1 L)\left(4K_1 n_1^3 n_2 - 6 n_1^5 n_2 - 4K_1 n_1 n_2^3 + 20 n_1^3 n_2^3 - 6 n_1 n_2^5\right) + \\ \cos(n_2 L)\sinh(n_1 L)\left(-K_1 n_1^4 + n_1^6 + 6K_1 n_1^2 n_2^2 - 15 n_1^4 n_2^2 - K_1 n_2^4 + 15 n_1^2 n_2^4 - n_2^6 + \frac{E_a (h_1 + t) K_2}{2t(1-\nu_a^2) D_1}\right),$$

$$a_{66} = -\cos(n_2 L)\cosh(n_1 L)\left(4K_1 n_1^3 n_2 - 6 n_1^5 n_2 - 4K_1 n_1 n_2^3 + 20 n_1^3 n_2^3 - 6 n_1 n_2^5\right) + \\ \sin(n_2 L)\sinh(n_1 L)\left(-K_1 n_1^4 + n_1^6 + 6K_1 n_1^2 n_2^2 - 15 n_1^4 n_2^2 - K_1 n_2^4 + 15 n_1^2 n_2^4 - n_2^6 + \frac{E_a (h_1 + t) K_2}{2t(1-\nu_a^2) D_1}\right),$$

$$a_{67} = \frac{E_a (h_1 + t) K_2}{2t(1-\nu_a^2) D_1}, \quad a_{68} = 0, \quad b_6 = 0;$$

$$a_{71} = \frac{\sinh(m_1 L)}{m_1}, \quad a_{72} = \frac{\cosh(m_1 L) - 1}{m_1}, \quad a_{73} = \frac{n_1 \cos(n_2 L)\sinh(n_1 L) + n_2 \sin(n_2 L)\cosh(n_1 L)}{n_1^2 + n_2^2},$$

$$a_{74} = \frac{n_1 \sin(n_2 L)\sinh(n_1 L) + n_2\left(1 - \cos(n_2 L)\cosh(n_1 L)\right)}{n_1^2 + n_2^2},$$

$$a_{75} = \frac{n_1\left(-1 + \cos(n_2 L)\cosh(n_1 L)\right) + n_2 \sin(n_2 L)\sinh(n_1 L)}{n_1^2 + n_2^2},$$

$$a_{76} = \frac{n_1 \sin(n_2 L)\cosh(n_1 L) - n_2 \cos(n_2 L)\sinh(n_1 L)}{n_1^2 + n_2^2}, \quad a_{77} = L, \quad a_{78} = 0, \quad b_7 = -P/2;$$

$$a_{81} = \frac{\left(\sinh(m_1 L) - m_1 L \cosh(m_1 L)\right)\left(-K_1 + m_1^2\right)}{K_2 m_1},$$

$$a_{82} = \frac{\left(-1 + \cosh(m_1 L) - m_1 L \sinh(m_1 L)\right)\left(-K_1 + m_1^2\right)}{K_2 m_1},$$

$$a_{83} = \frac{1}{K_2\left(n_1^2 + n_2^2\right)}\Big\{K_1\Big[-n_1 \cos(n_2 L)\sinh(n_1 L) + n_1^2 L \cos(n_2 L)\cosh(n_1 L) + n_2 \cosh(n_1 L)\left(-\sin(n_2 L) + n_2 L \cos(n_2 L)\right)\Big] + \left(n_1^2 + n_2^2\right)\Big[-L n_1^2 \cos(n_2 L)\cosh(n_1 L) + n_2 \cosh(n_1 L)\left(-\sin(n_2 L) + n_2 L \cos(n_2 L)\right) + n_1 \sinh(n_1 L)\left(\cos(n_2 L) + 2 n_2 L \sin(n_2 L)\right)\Big]\Big\},$$

$$a_{84} = \frac{1}{K_2\left(n_1^2 + n_2^2\right)}\Big\{K_1\Big[-n_1 \sin(n_2 L)\sinh(n_1 L) + n_1^2 L \sin(n_2 L)\cosh(n_1 L) + n_2\left(-1 + \cos(n_2 L)\cosh(n_1 L) + n_2 L \sin(n_2 L)\cosh(n_1 L)\right)\Big] + \left(n_1^2 + n_2^2\right)\Big[-L n_1^2 \sin(n_2 L)\cosh(n_1 L) + n_1 \sinh(n_1 L)\left(\sin(n_2 L) - 2 n_2 L \cos(n_2 L)\right) + n_2\left(-1 + \cos(n_2 L)\cosh(n_1 L) + n_2 L \sin(n_2 L)\cosh(n_1 L)\right)\Big]\Big\},$$

$$a_{85} = \frac{1}{K_2\left(n_1^2 + n_2^2\right)}\Big\{K_1\Big[n_1\left(1 - \cos(n_2 L)\cosh(n_1 L)\right) + n_1^2 L \cos(n_2 L)\sinh(n_1 L) + n_2 \sinh(n_1 L)\left(-\sin(n_2 L) + n_2 L \cos(n_2 L)\right)\Big] - \left(n_1^2 + n_2^2\right)\Big[n_1^2 L \cos(n_2 L)\sinh(n_1 L) + n_2 \sinh(n_1 L)\left(\sin(n_2 L) - n_2 L \cos(n_2 L)\right) - n_1\left(-1 + \cos(n_2 L)\cosh(n_1 L) + 2 n_2 L \sin(n_2 L)\cosh(n_1 L)\right)\Big]\Big\},$$

$$a_{86} = \frac{1}{K_2\left(n_1^2 + n_2^2\right)}\Big\{K_1\Big[-n_1 \sin(n_2 L)\cosh(n_1 L) + n_1^2 L \sin(n_2 L)\sinh(n_1 L) + n_2 \sinh(n_1 L)\left(\cos(n_2 L) + n_2 L \sin(n_2 L)\right)\Big] + \left(n_1^2 + n_2^2\right)\Big[-L n_1^2 \sin(n_2 L)\sinh(n_1 L) + n_1 \cosh(n_1 L)\left(\sin(n_2 L) - 2 n_2 L \cos(n_2 L)\right) + n_2 \sinh(n_1 L)\left(\cos(n_2 L) + n_2 L \sin(n_2 L)\right)\Big]\Big\},$$

$$a_{87} = 0, \quad a_{88} = -1, \quad b_8 = \frac{h_1 + t}{2}\frac{P}{2}.$$

Table 1. Comparison of the stress peaks given by the solution developed in this paper (this sol.) and the Volkersen's solution (Volk. sol.) with finite element models (FE), for all cases of adhesive thickness (t) and overlap length (L); elastic modulus ratio $E_{adher} / E_{adhes} = 100$.

t (mm)		**0.25**			**0.50**		
L (mm)		**10**	**30**	**50**	**10**	**30**	**50**
σ_{peak} left (MPa)	this sol.	-0.786	-1.328	-2.123	-0.763	-1.023	-1.517
	Volk. sol.	-0.773	-1.185	-1.649	-0.746	-0.949	-1.252
	FE	-0.692	-1.138	-1.815	-0.649	-0.869	-1.285
	$\Delta_{t.s.-FE}$ %	13.5%	16.6%	17.0%	17.6%	17.7%	18.0%
	$\Delta_{Volk.-FE}$ %	11.7%	4.1%	-9.1%	14.9%	9.3%	-2.6%
σ_{peak} right (MPa)	this sol.	0.786	1.328	2.123	0.763	1.023	1.517
	Volk. sol.	0.773	1.185	1.649	0.746	0.949	1.252
	FE	0.776	1.279	2.039	0.688	0.911	1.343
	$\Delta_{t.s.-FE}$ %	1.3%	3.8%	4.1%	11.0%	12.2%	12.9%
	$\Delta_{Volk.-FE}$ %	-0.4%	-7.4%	-19.1%	8.4%	4.2%	-6.8%
τ_{peak} left (MPa)	this sol.	-1.101	-1.957	-3.148	-1.046	-1.516	-2.280
	Volk. sol.	-1.091	-1.870	-2.652	-1.044	-1.455	-2.119
	FE	-1.116	-1.952	-3.132	-1.076	-1.522	-2.275
	$\Delta_{t.s.-FE}$ %	-1.3%	0.3%	0.5%	-2.8%	-0.4%	0.2%
	$\Delta_{Volk.-FE}$ %	-2.2%	-4.2%	-15.3%	-3.0%	-4.5%	-6.9%
τ_{peak} right (MPa)	this sol.	-1.101	-1.957	-3.148	-1.046	-1.516	-2.280
	Volk. sol.	-1.091	-1.870	-2.652	-1.044	-1.455	-2.119
	FE	-1.150	-2.006	-3.219	-1.092	-1.542	-2.306
	$\Delta_{t.s.-FE}$ %	-4.2%	-2.4%	-2.2%	-4.2%	-1.7%	-1.1%
	$\Delta_{Volk.-FE}$ %	-5.1%	-6.8%	-17.6%	-4.4%	-5.7%	-8.1%

Table 2. Comparison of the stress peaks given by the solution developed in this paper (this sol.) and the Volkersen's solution (Volk. sol.) with finite element models (FE), for all cases of adhesive thickness (t) and overlap length (L); elastic modulus ratio $E_{adher} / E_{adhes} = 20$.

t (mm)		**0.25**			**0.50**		
L (mm)		**10**	**20**	**30**	**10**	**20**	**30**
σ_{peak} left (MPa)	this sol.	-1.465	-2.595	-3.870	-1.228	-1.906	-2.771
	Volk. sol.	-1.441	-2.168	-2.904	-1.193	-1.650	-2.122
	FE	-0.978	-1.661	-2.468	-0.901	-1.350	-1.952
	$\Delta_{t.s.-FE}$ %	49.8%	56.2%	56.8%	36.4%	41.1%	41.9%
	$\Delta_{Volk.-FE}$ %	47.4%	30.5%	17.6%	32.4%	22.2%	8.7%
σ_{peak} right (MPa)	this sol.	1.465	2.595	3.870	1.228	1.906	2.771
	Volk. sol.	1.441	2.168	2.904	1.193	1.650	2.122
	FE	1.362	2.315	3.440	1.042	1.537	2.216
	$\Delta_{t.s.-FE}$ %	7.6%	12.1%	12.5%	17.8%	24.0%	25.0%
	$\Delta_{Volk.-FE}$ %	5.8%	-6.3%	-15.6%	14.4%	7.3%	-4.3%
τ_{peak} left (MPa)	this sol.	-1.510	-2.737	-4.086	-1.252	-2.007	-2.935
	Volk. sol.	-1.408	-2.356	-3.225	-1.201	-1.812	-2.370
	FE	-1.282	-2.270	-3.383	-1.135	-1.751	-2.547
	$\Delta_{t.s.-FE}$ %	17.8%	20.6%	20.8%	10.3%	14.6%	15.2%
	$\Delta_{Volk.-FE}$ %	9.9%	3.8%	-4.7%	5.9%	3.4%	-6.9%
τ_{peak} right (MPa)	this sol.	-1.510	-2.737	-4.086	-1.252	-2.007	-2.935
	Volk. sol.	-1.408	-2.356	-3.225	-1.201	-1.812	-2.370
	FE	-1.475	-2.595	-3.864	-1.231	-1.899	-2.759
	$\Delta_{t.s.-FE}$ %	2.3%	5.5%	5.7%	1.7%	5.7%	6.4%
	$\Delta_{Volk.-FE}$ %	-4.6%	-9.2%	-16.6%	-2.4%	-4.6%	-14.1%

Table 3. Comparison of the stress peaks given by the solution developed in this paper (this sol.) and the Volkersen's solution (Volk. sol.) with finite element models (FE), for all cases of adhesive thickness (t) and overlap length (L); elastic modulus ratio $E_{adher} / E_{adhes} = 5$.

t (mm)		**0.25**			**0.50**		
L (mm)		**10**	**20**	**30**	**10**	**20**	**30**
σ_{peak} left (MPa)	this sol.	-3.094	-6.142	-9.280	-2.326	-4.458	-6.682
	Volk. sol.	-2.969	-5.112	-7.259	-2.168	-3.413	-4.670
	FE	-1.269	-2.472	-3.706	-1.391	-2.693	-4.038
	$\Delta_{t.s.-FE}$ %	143.8%	148.5%	150.4%	67.2%	65.6%	65.5%
	$\Delta_{Volk.-FE}$ %	134.0%	106.8%	95.9%	55.9%	26.7%	15.6%
σ_{peak} right (MPa)	this sol.	3.094	6.142	8.992	2.326	4.458	6.683
	Volk. sol.	2.969	5.112	7.259	2.168	3.413	4.670
	FE	2.337	4.542	6.813	1.573	2.888	4.324
	$\Delta_{t.s.-FE}$ %	32.4%	35.2%	32.0%	47.8%	54.4%	54.5%
	$\Delta_{Volk.-FE}$ %	27.1%	12.6%	6.6%	37.8%	18.2%	8.0%
τ_{peak} left (MPa)	this sol.	-2.534	-5.041	-7.587	-1.868	-3.619	-5.426
	Volk. sol.	-1.694	-4.269	-3.346	-1.562	-2.874	-5.137
	FE	-1.507	-2.966	-4.448	-1.263	-2.376	-3.560
	$\Delta_{t.s.-FE}$ %	68.1%	70.0%	70.6%	48.0%	52.3%	52.4%
	$\Delta_{Volk.-FE}$ %	12.4%	43.9%	-24.8%	23.7%	21.0%	44.3%
τ_{peak} right (MPa)	this sol.	-2.534	-5.041	-7.504	-1.868	-3.619	-5.427
	Volk. sol.	-1.694	-4.269	-3.346	-1.562	-2.874	-5.137
	FE	-2.089	-4.096	-6.143	-1.572	-2.948	-4.416
	$\Delta_{t.s.-FE}$ %	21.3%	23.1%	22.2%	18.9%	22.8%	22.9%
	$\Delta_{Volk.-FE}$ %	-18.9%	4.2%	-45.5%	-0.6%	-2.5%	16.3%

Table 4. Results from the strain gauges in the unbonded zone of the gusset and theoretical value corresponding to a tensile loading of 30 N/mm.

Outer surface, mid-span gauge	Outer surface, quarter-span gauge	Inner surface, mid-span gauge	Inner surface, quarter-span gauge	Theoretical (tension)
$8.4 \cdot 10^{-5}$	$9.0 \cdot 10^{-5}$	$8.9 \cdot 10^{-5}$	$8.7 \cdot 10^{-5}$	$8.9 \cdot 10^{-5}$

Table 5. Comparison of the stress peaks given by the solution developed in this paper (this sol.) and finite element models (FE),

t (mm)	**0.25**	L (mm)	**30**
E_1h_1 / E_2h_2		**0.4**	**2.3**
E_1 / E_a		19.2	33.7
E_2 / E_a		33.7	19.2
σ_{peak} left	this sol.	-4.70	-1.67
	FE	-3.30	-1.11
	$\Delta_{t.s.-FE}$ %	42.5%	49.5%
σ_{peak} right	this sol.	1.98	3.96
	FE	1.826	3.69
	$\Delta_{t.s.-FE}$ %	8.4%	7.3%
τ_{peak} left	this sol.	-4.79	-2.08
	FE	-4.17	-1.77
	$\Delta_{t.s.-FE}$ %	14.7%	17.3%
τ_{peak} right	this sol.	-2.01	-4.94
	FE	-1.94	-4.77
	$\Delta_{t.s.-FE}$ %	3.8%	3.6%

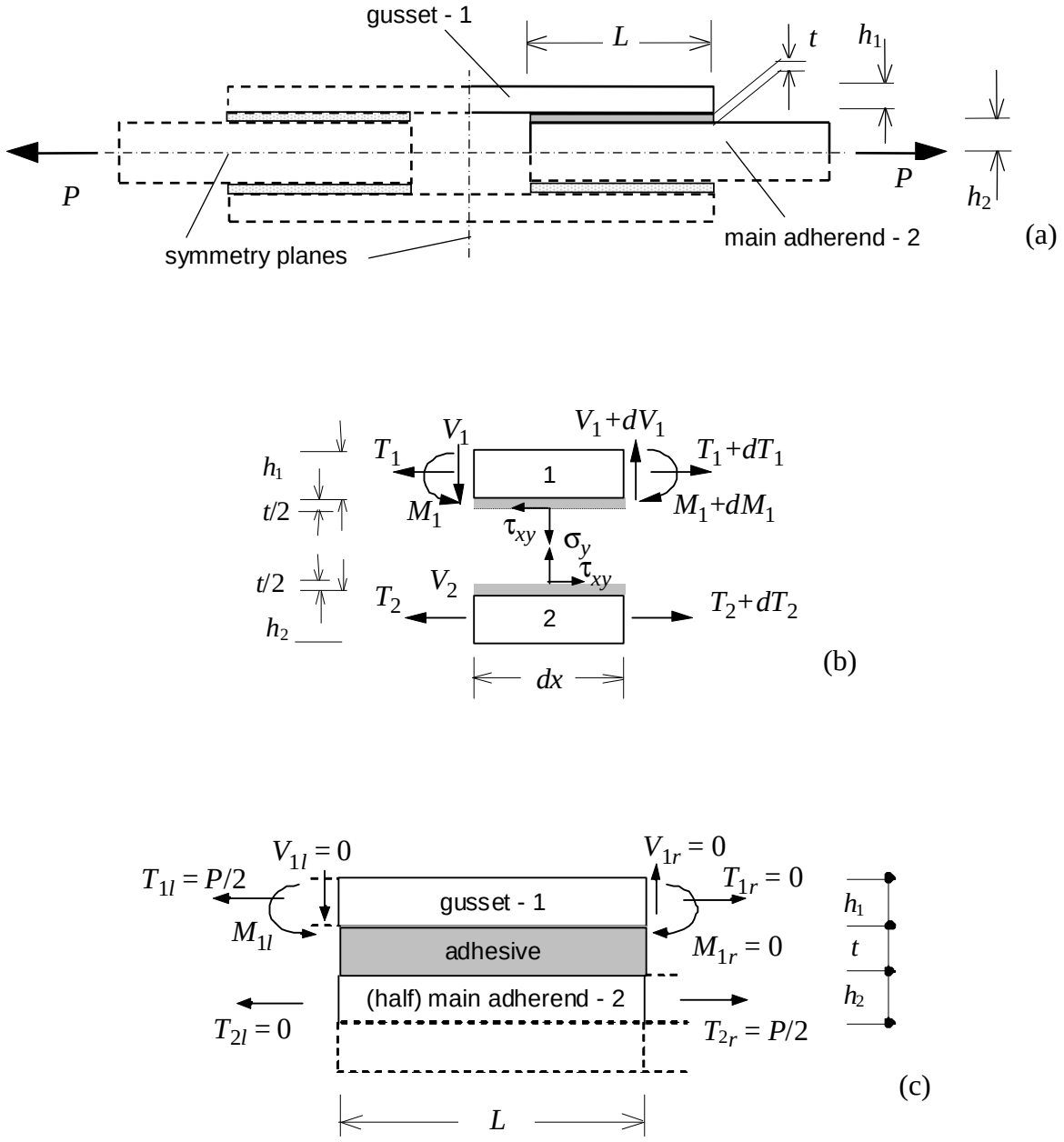

Figure 1. Double lap joint: a) dimensions and symmetry conditions; b) infinitesimal equilibrium; c) boundary conditions.

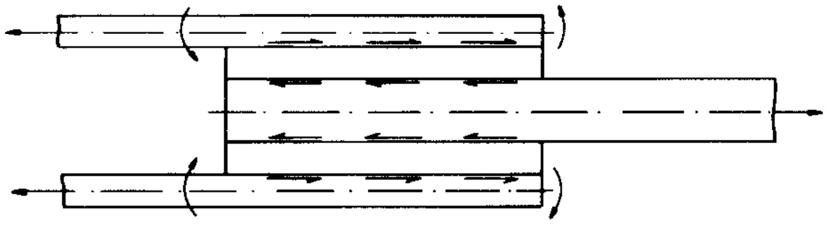

Figure 2. Bending action on the gussets of a double lap joint (from [26], copyright Elsevier).

a)

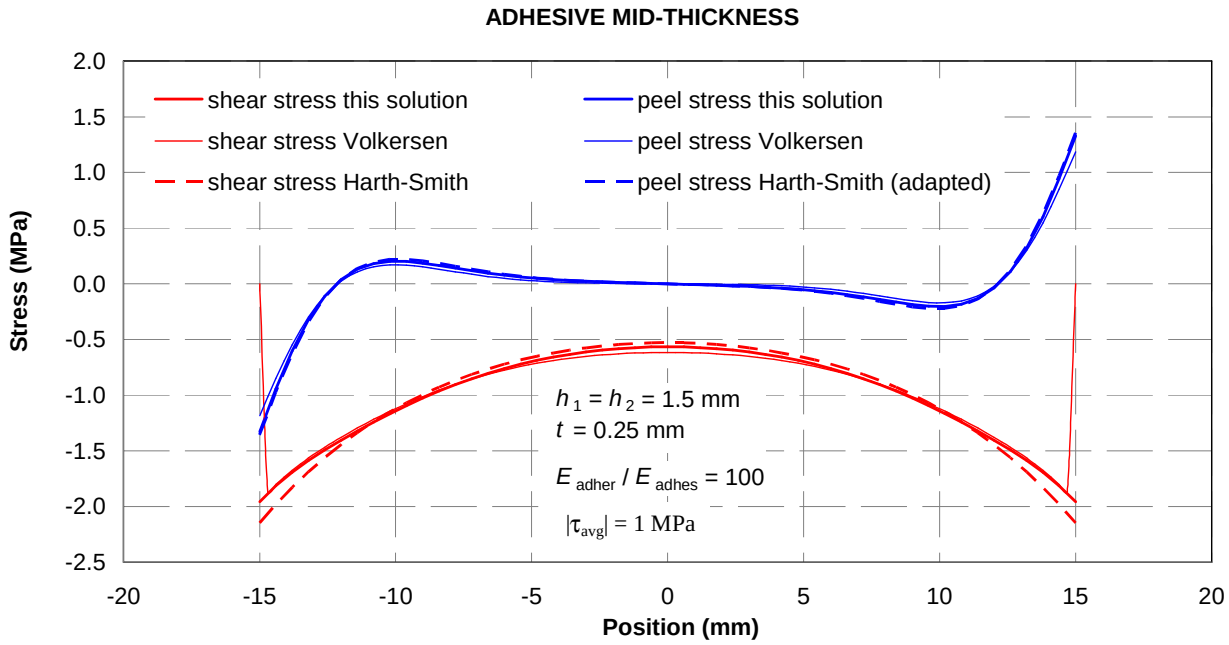
ADHESIVE MID-THICKNESS
shear stress this solution
shear stress Volkersen
shear stress Harth-Smith
peel stress this solution
peel stress Volkersen
peel stress Harth-Smith (adapted)
h 1 = h 2 = 1.5 mm
t = 0.25 mm
E adher / E adhes = 100
|τavg| = 1 MPa
Stress (MPa)
Position (mm)
2.0
1.5
1.0
0.5
0.0
-0.5
-1.0
-1.5
-2.0
-2.5
-20
-15
-10
-5
0
5
10
15
20

b)

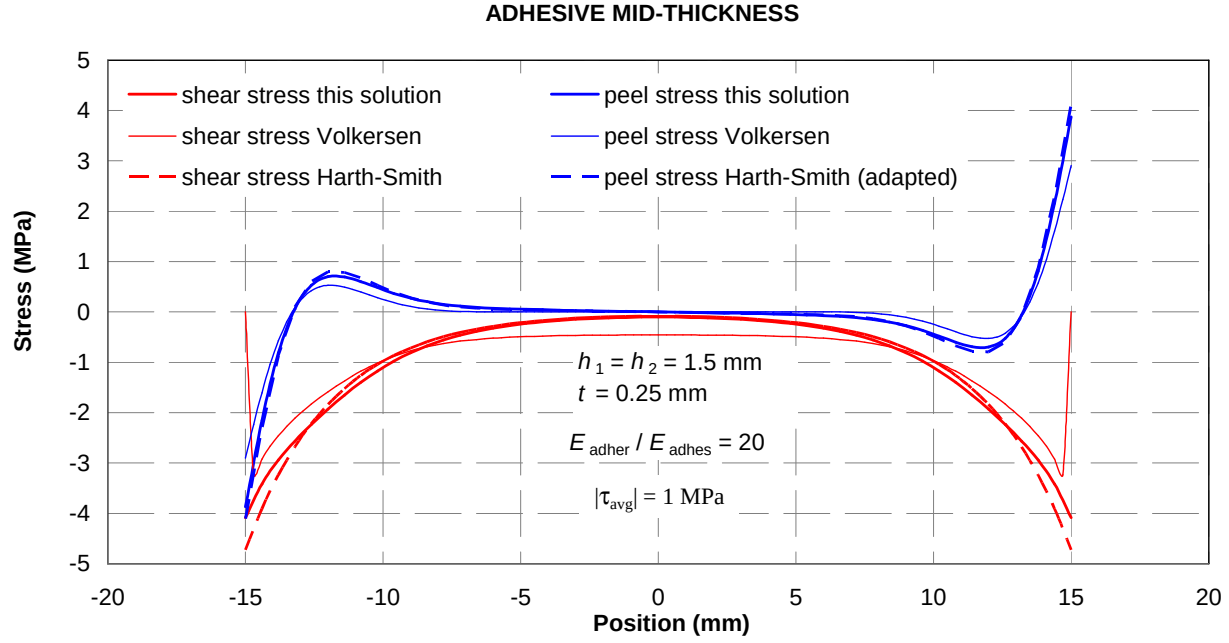
ADHESIVE MID-THICKNESS
shear stress this solution
shear stress Volkersen
shear stress Harth-Smith
peel stress this solution
peel stress Volkersen
peel stress Harth-Smith (adapted)
h 1 = h 2 = 1.5 mm
t = 0.25 mm
E adher / E adhes = 20
|τavg| = 1 MPa
Stress (MPa)
Position (mm)
5
4
3
2
1
0
-1
-2
-3
-4
-5
-20
-15
-10
-5
0
5
10
15
20

c)

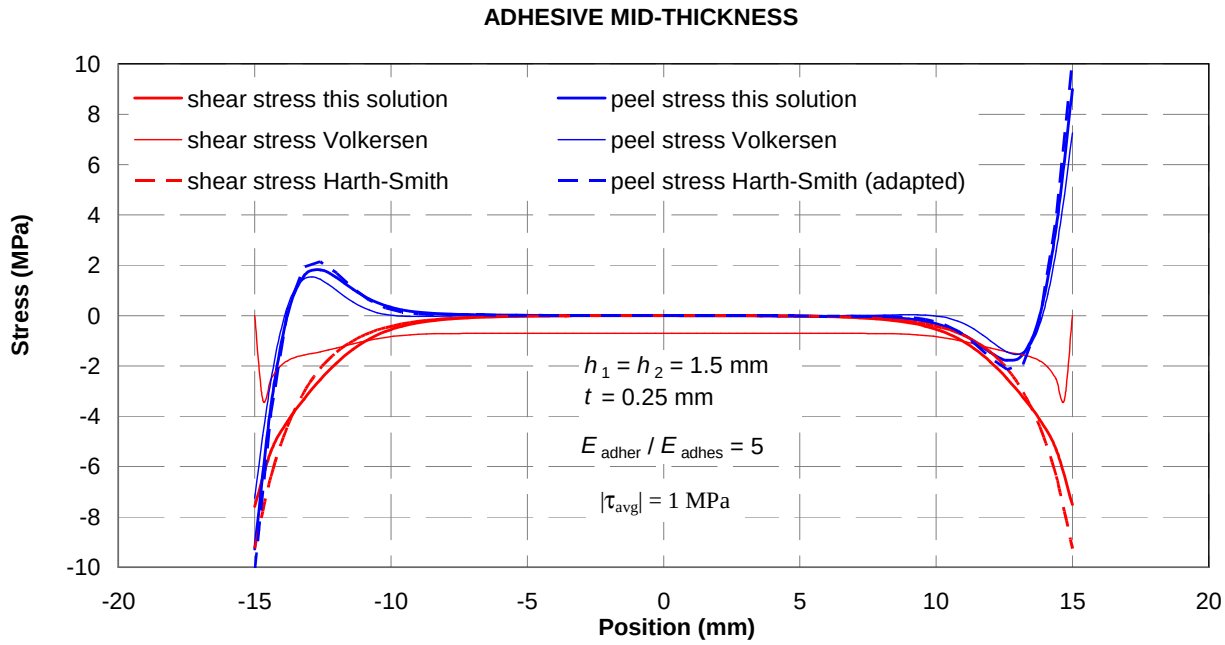

Figure 3. Stress distribution in a double lap joint; comparison between present, Volkersen's and Hart-Smith's solutions for three different materials of the adherends: a) "stiff"; b) "intermediate"; c) "soft".

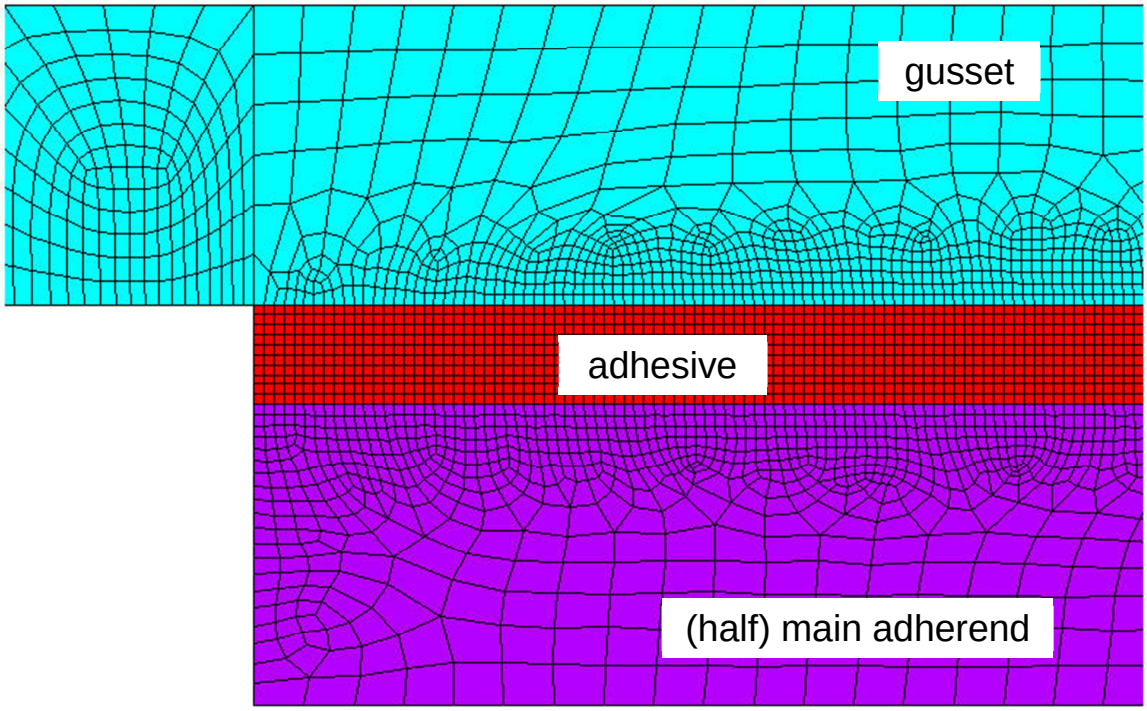

Figure 4. Detail of the mesh of a finite element model used for comparison.

a)

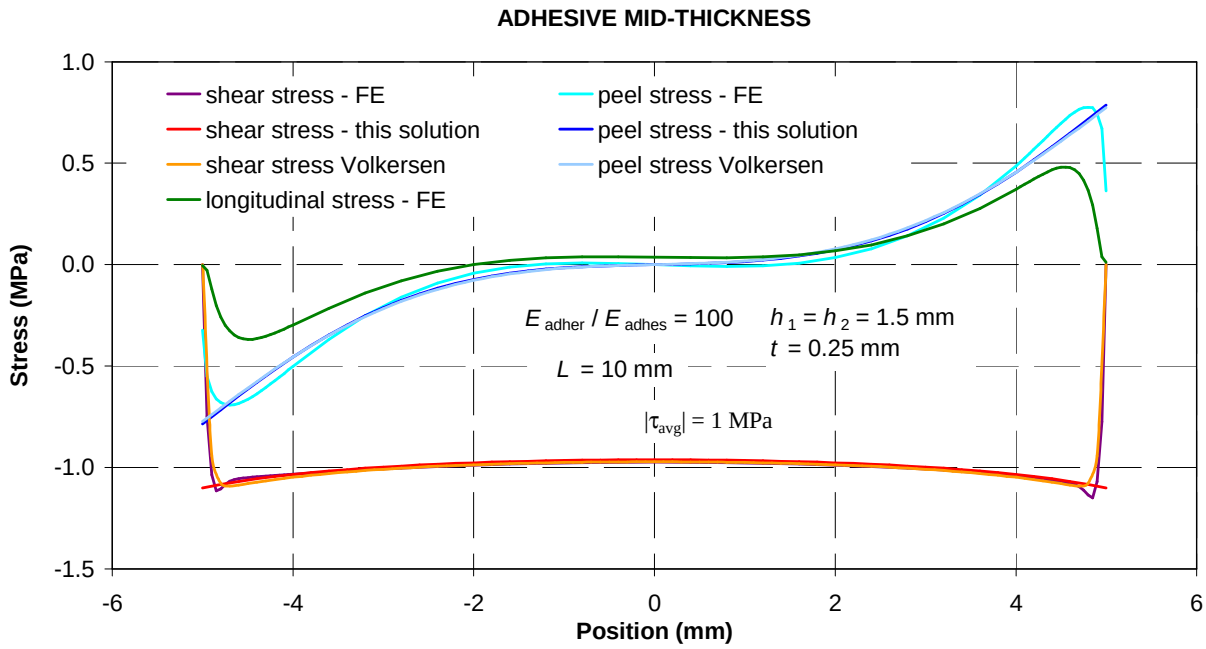
ADHESIVE MID-THICKNESS
shear stress - FE
shear stress - this solution
shear stress Volkersen
longitudinal stress - FE
peel stress - FE
peel stress - this solution
peel stress Volkersen
E adher / E adhes = 100
h 1 = h 2 = 1.5 mm
t = 0.25 mm
L = 10 mm
|τavg| = 1 MPa
Stress (MPa)
Position (mm)
1.0
0.5
0.0
-0.5
-1.0
-1.5
-6
-4
-2
0
2
4
6

b)

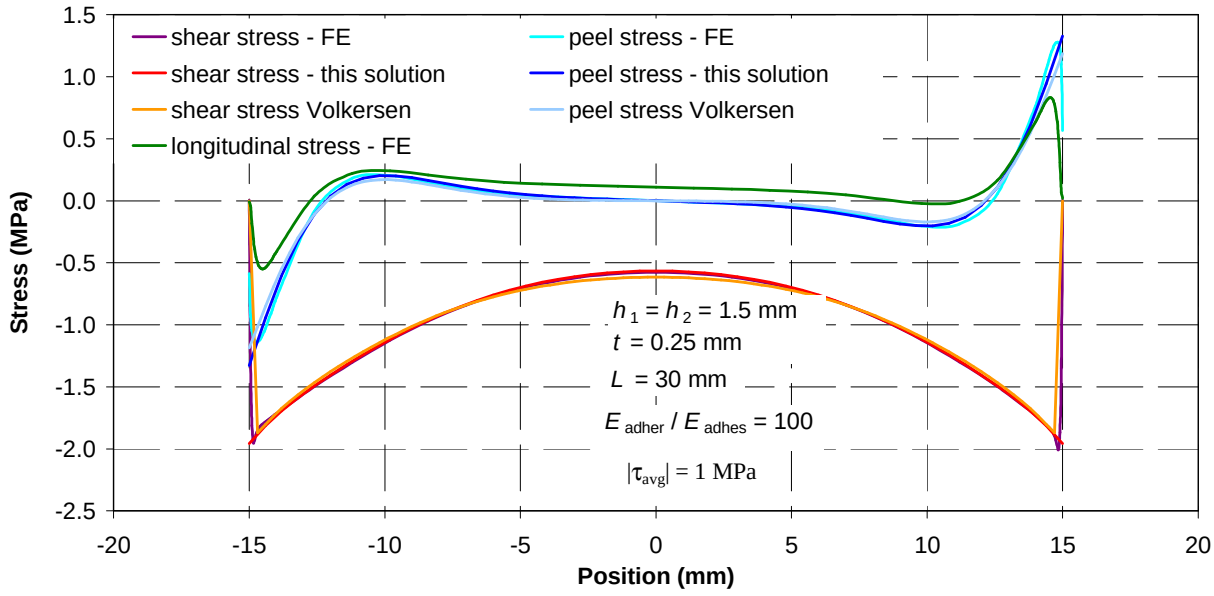
ADHESIVE MID-THICKNESS
shear stress - FE
shear stress - this solution
shear stress Volkersen
longitudinal stress - FE
peel stress - FE
peel stress - this solution
peel stress Volkersen
h 1 = h 2 = 1.5 mm
t = 0.25 mm
L = 30 mm
E adher / E adhes = 100
|τavg| = 1 MPa
Stress (MPa)
Position (mm)
1.5
1.0
0.5
0.0
-0.5
-1.0
-1.5
-2.0
-2.5
-20
-15
-10
-5
0
5
10
15
20

c)

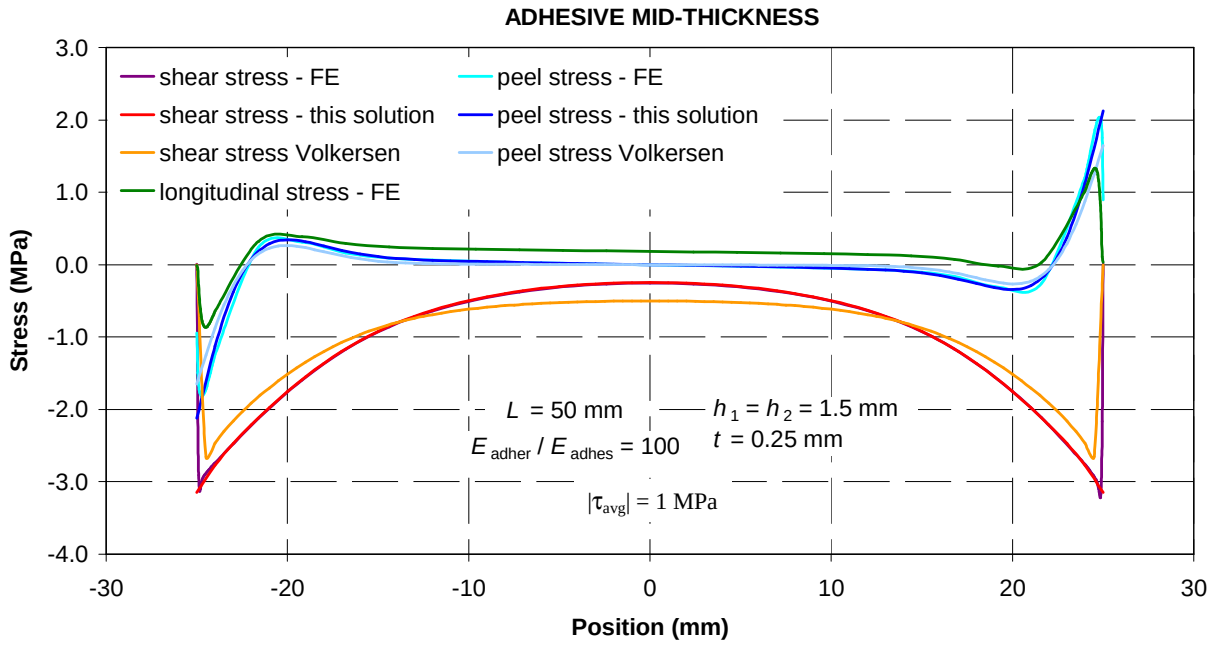

Figure 5. Stress distribution in a double lap joint, case of a "stiff" material of the adherends; comparison between finite element results and present solution for three different overlap lengths: a) 10 mm; b) 30 mm; c) 50 mm.

a)

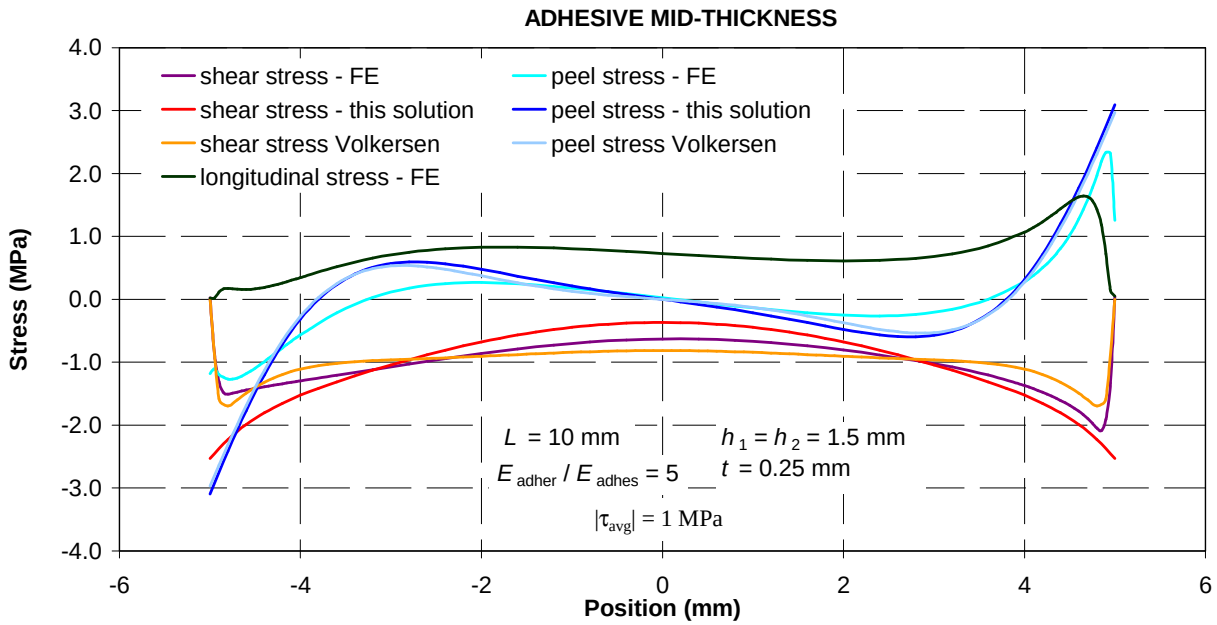
ADHESIVE MID-THICKNESS
shear stress - FE
shear stress - this solution
shear stress Volkersen
longitudinal stress - FE
peel stress - FE
peel stress - this solution
peel stress Volkersen
Stress (MPa)
Position (mm)
L = 10 mm
h1 = h2 = 1.5 mm
E adher / E adhes = 5
t = 0.25 mm
|τavg| = 1 MPa

b)

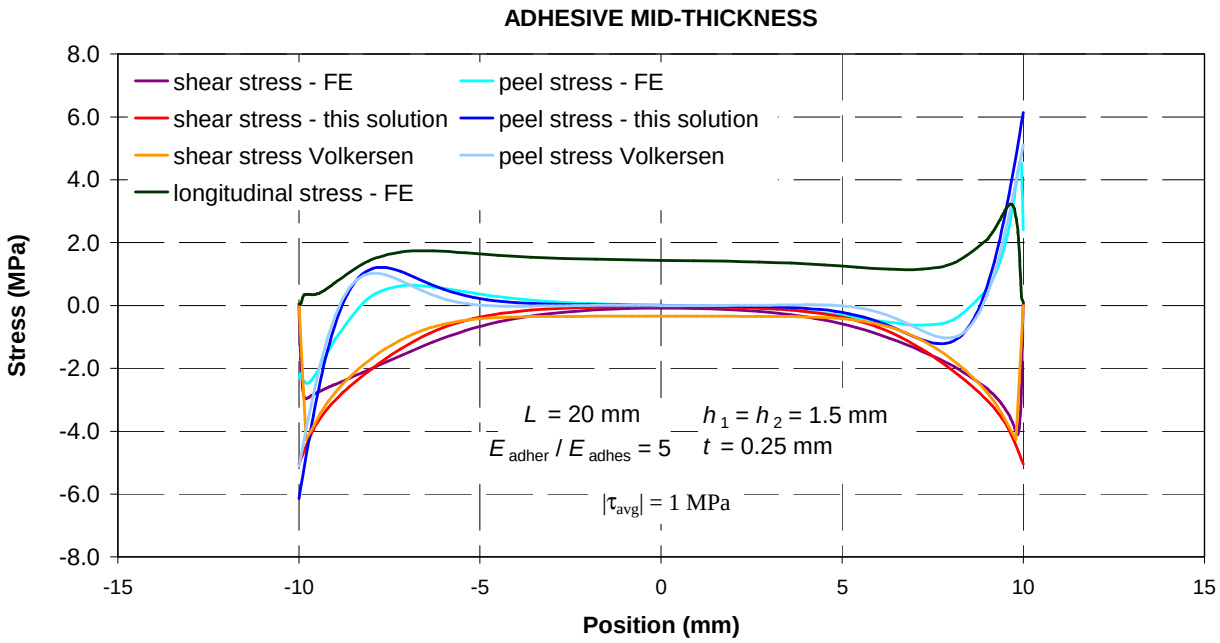
ADHESIVE MID-THICKNESS
shear stress - FE
shear stress - this solution
shear stress Volkersen
longitudinal stress - FE
peel stress - FE
peel stress - this solution
peel stress Volkersen
Stress (MPa)
Position (mm)
L = 20 mm
h1 = h2 = 1.5 mm
E adher / E adhes = 5
t = 0.25 mm
|τavg| = 1 MPa

c)

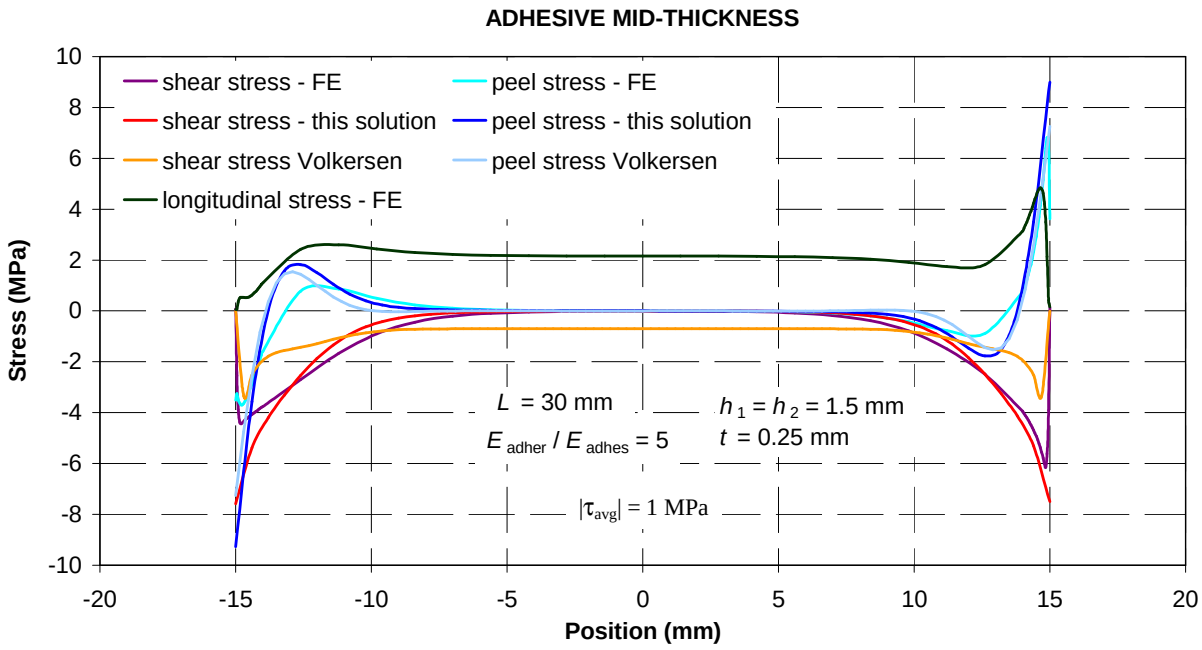

Figure 6. Stress distribution a double lap joint, case of a "soft" material of the adherends; comparison between finite element results and present solution for three different overlap lengths: a) 10 mm; b) 20 mm; c) 30 mm.

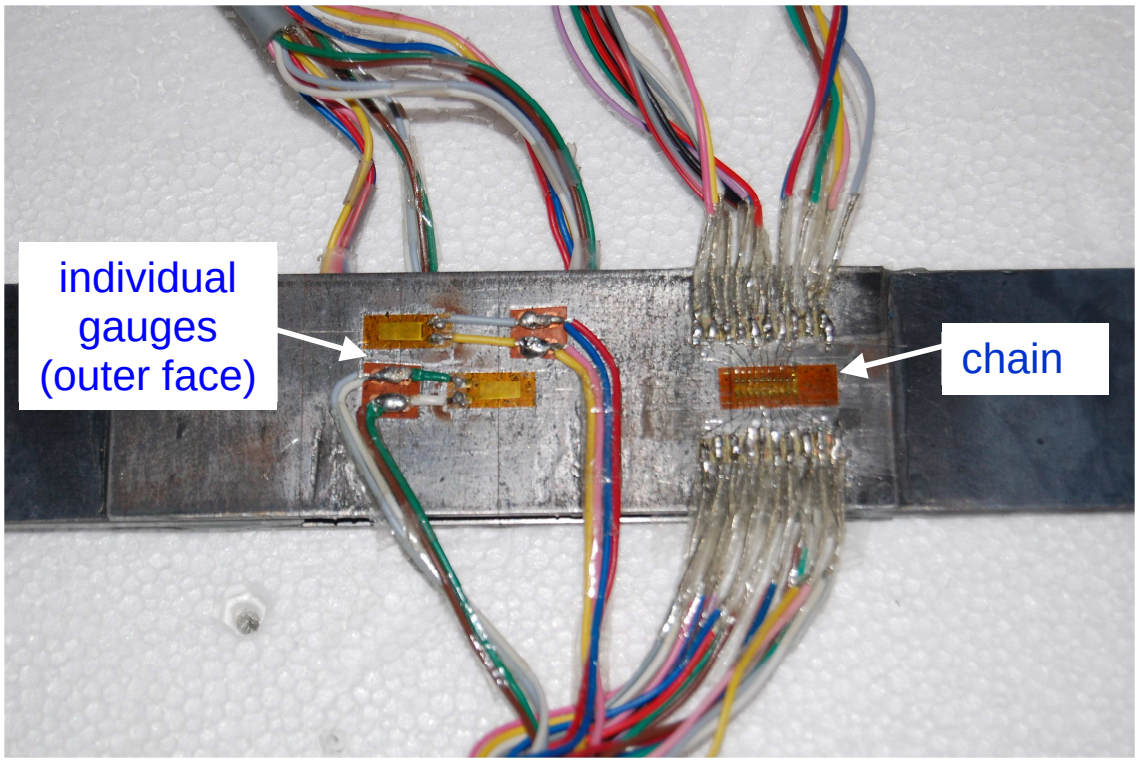

Figure 7. Strain gauge installation on a double lap joint.

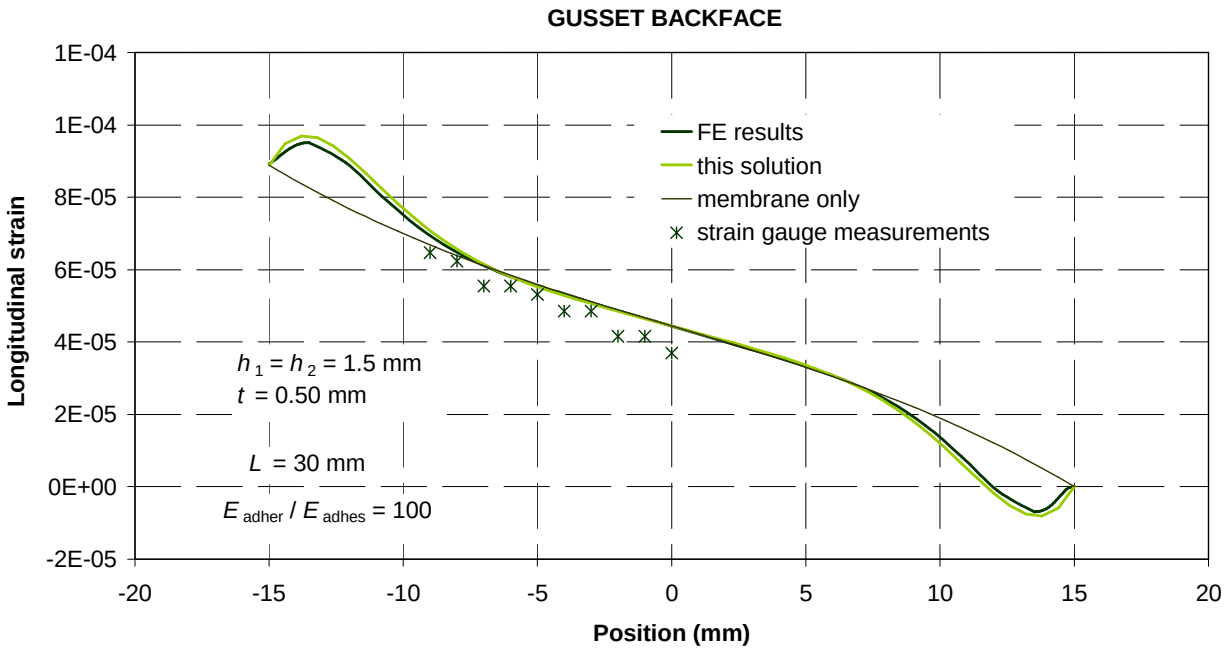

Figure 8. Longitudinal strain in the back face of the gusset.

a)

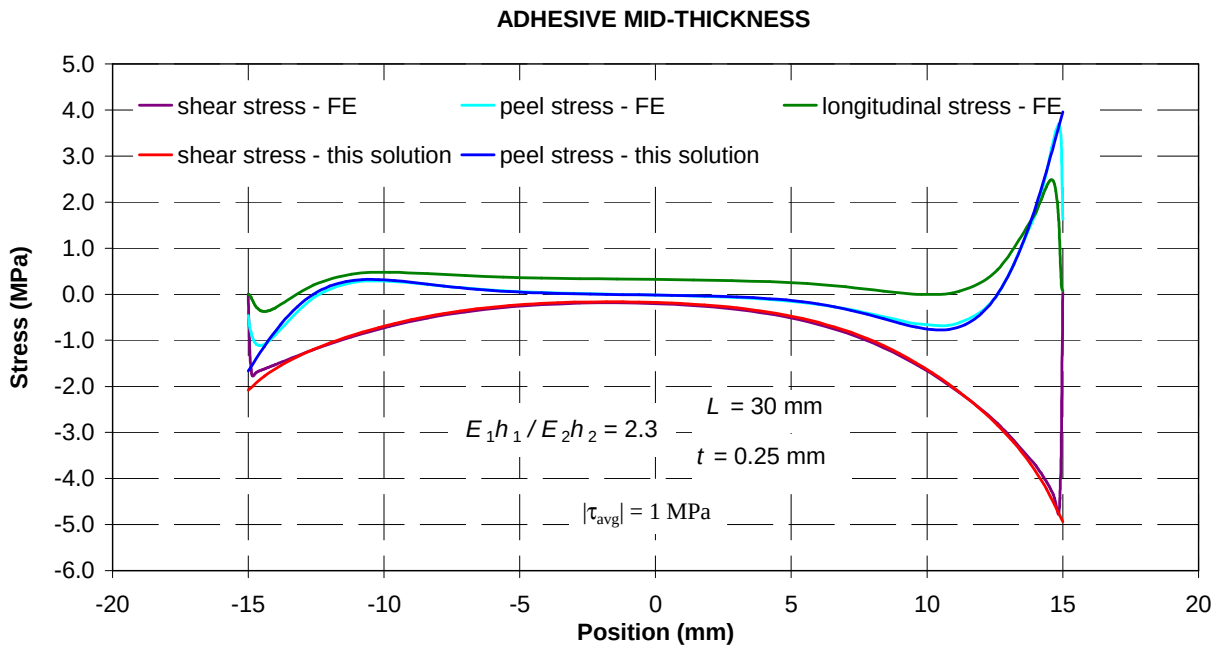

b)

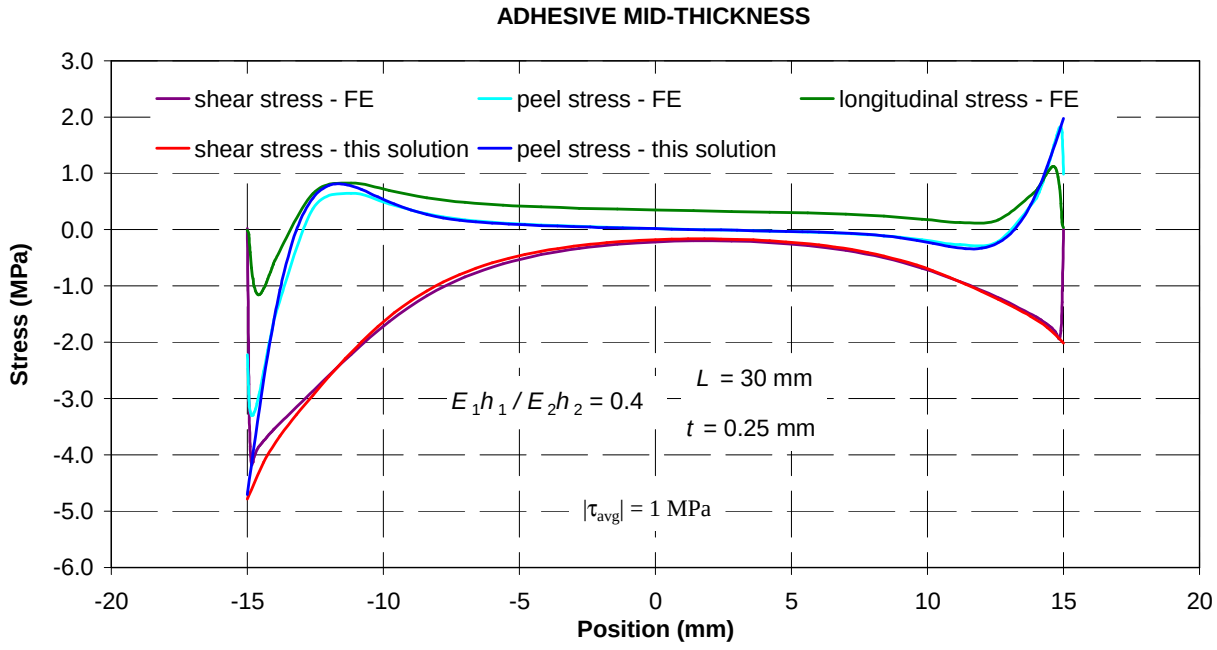

Figure 9. Stress distribution in an unbalanced double lap joint, comparison between finite element results and present solution for two different stiffness ratios E_1h_1/E_2h_2: a) 2.3; b) 0.4.